Accepted in Chemosphere on 4th March 2022

Prospects of MXenes in energy storage applications

P. E. Lokhande[1,2], Amir Pakdel[2], H. M. Pathan[1], Deepak Kumar[3], Dai-Viet N. Vo[4], Adel Al-Gheethi[5], Ajit Sharma[3], Saurav Goel[6,7,8], Prabal Pratap Singh[9] and Byeong-Kyu Lee[10]

[1]Department of Physics, Savitribai Phule Pune University, Pune, 411007, India

[2]Department of Mechanical, Manufacturing and Biomedical Engineering, Trinity College Dublin, Dublin, Ireland

[3]School of Chemical Engineering and Physical Sciences, Lovely Professional University, Phagwara, 144411, India

[4]Center of Excellence for Green Energy and Environmental Nanomaterials (CE@GrEEN), Nguyen Tat Thanh University, Ho Chi Minh City 755414, Vietnam

[5]Faculty of Civil Engineering and Built Environment (FKAAB), Universiti Tun Hussein Onn Malaysia (UTHM), 86400, Batu Pahat, Johor Malaysia

[6]School of Engineering, London South Bank University, London, SE1 0 AA, UK

[7]University of Petroleum and Energy Studies, Dehradun, 248007, India

[8]Indian Institute of Technology Guwahati, Guwahati, 781039, India

[9]Department of Chemistry, GLA University, Mathura, India

[10]Department of Civil and Environmental Engineering, University of Ulsan, Daehak, Korea

Corresponding author: prasadlokhande2007@gmail.com, deepak.sharma99967@gmail.com

Abstract

The transition metal carbides/nitrides referred to as MXenes has emerged as a wonder material presenting newer opportunities owing to their unique properties such as high thermal and electrical conductivity, high negative zeta-potential and mechanical properties similar to the parent transition metal carbides/nitrides. These properties of MXenes can be utilized in various societal applications including for energy storage and energy conversion. In this focused review, we provide a ready glance into the evolutionary development of the MXene family and various efforts that are made globally towards property improvement and performance enhancement. Particular attention in this review is made to direct the attention of readers to the bright prospects of MXene in the energy storage and energy conversion process – which is extremely timely to tackle the current concern on climate change. The review concludes by offering fresh insights into the future research needs and challenges that need to be addressed to develop resilient energy solutions.

Keywords: MXene; 2D materials, Energy storage; Supercapacitor; Li-ion battery

1. Introduction

The discovery of unique properties in single-layered graphene has led to a major research focus on two-dimensional (2D) materials [1–4]. The extraordinary properties of 2D materials such as mechanical, electrochemical, optical and electronic properties make them special for various applications in chemistry, medicine, nanotechnology, materials and engineering sciences [5,6]. Transition metal nitrides, carbides and carbonitrides are the new families of 2D materials also called Mxene which were discovered in 2011 at Drexel University by Gogotsi [7,8]. Unlike graphene, Mxenes involve transition metal dichalcogenides, boron nitride, layered oxides, black phosphorous, etc. and these have now started to shape a new avalanche of opportunities [9,10].

The general formula for MXene is $M_{n+1}X_nT_x$ (n = 1-3) where *M* stands for early transition metal such as Ti, Nb, Zr, V, Hf, Sc, Mo, Cr, etc., *X* is the carbon and/or nitrogen while T_x is the surface functional groups such as oxygen, hydroxyl, chlorine and/or fluorine bonded to the outer layers of M [11,12] as shown in **Figure 1**. A variety of structures and compositions are thus which has resulted in a massive expansion of MXene derivatives. **Figure 2** shows a wide variety of compositions researched and reported to date.

MXene materials are prepared by chemical selective etching of A elements from layered ternary material $M_{n+1}AX_n$ or called MAX phase wherein, A is the element belonging to group IIIA or IVA of the periodic table [7,13]. MXenes are being extensively researched due to their properties offering uniqueness like graphene. Firstly, both MXene and graphene materials are synthesized using a top-down exfoliation approach from their bulk precursor (MAX and graphite) where exfoliation enables the synthesis of large-scale two-dimensional materials having minimum thickness down to a single to few atomic layers along with extraordinary chemical and physical properties [14]. Secondly, both materials can be modified by tuning their morphology, surface properties and crystal structure.

For example, porosity and curvature of MXene and graphene can be modified through higher surface area and pore volume while their microstructure can be regulated by using heteroatom's doping. Thirdly both MXene and graphene have a higher specific surface area and excellent electrical conductivity which is beneficial for applications like energy storage devices. Due to these similarities Mxene offers great prospects in energy storage and conversion [15–21].

Beyond superior electric conductivity and higher surface area, MXene carries rich surface chemistry and other excellent properties due to the surface terminals groups (-OH, –O, -F). Due to these reasons, many other advantages of MXenes have emerged making them suitable for wider applications in areas ranging from energy storage devices [22–26], transparent conductor [27–30], electromagnetic interface shielding [31,32],

photo/electrocatalysis [33–36], catalyst [34,37], purifier [38,39], gas sensors [40], filler in polymeric composite [41], tribo-additives [42], dual response surfaces [43], substrate for dyes [44], methane storage [45], ceramic biomaterial for cancer therapy [46]. hydrogen storage [47,48] and nanoscale superconductivity [49] to name a few. Other avenues for Mxenes have also been explored using simulation approaches including applications in optical, electronic, sensing and thermoelectrics and catalytic reaction [38]–[41]

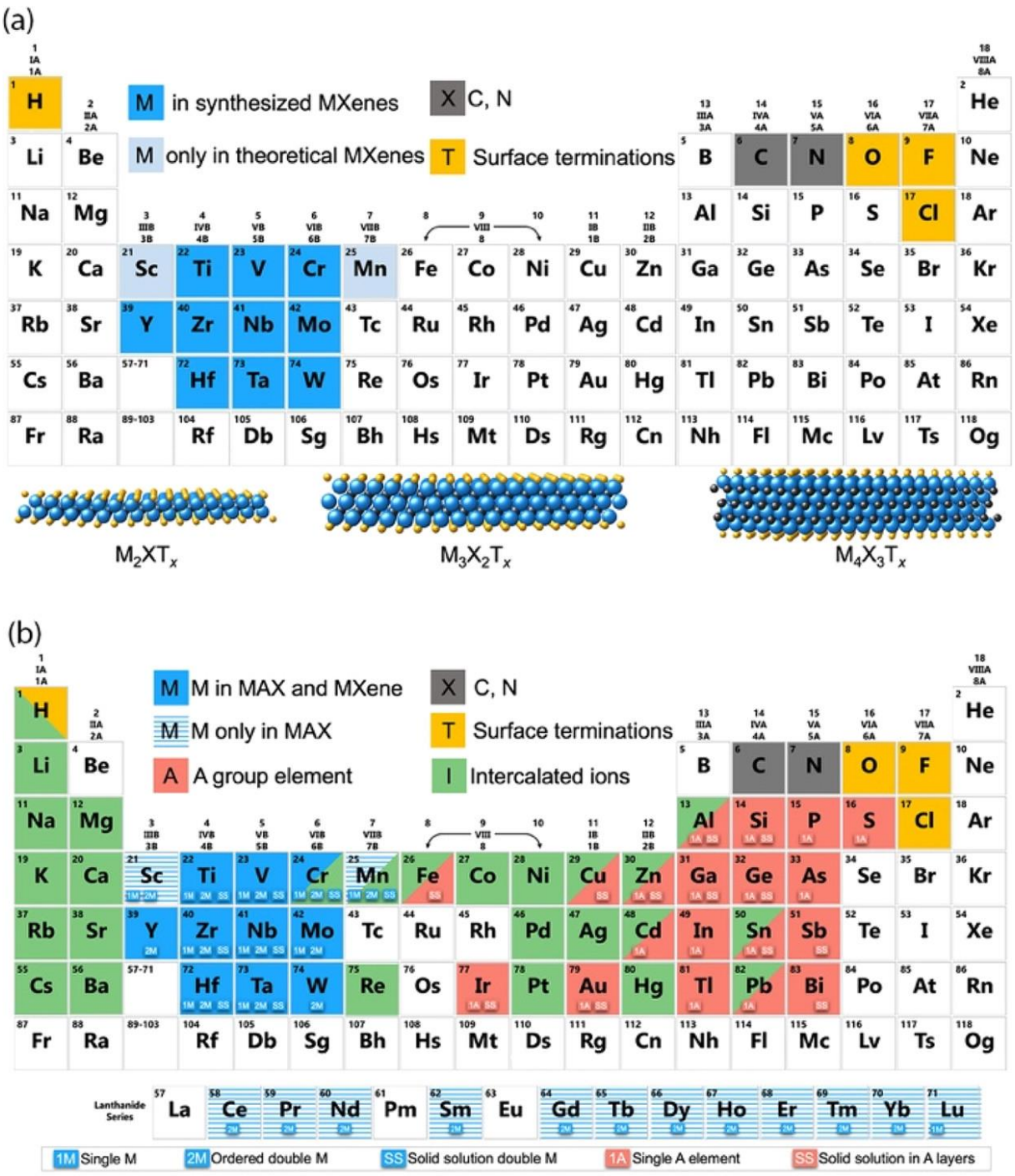

Figure 1: MXene compositions reported to date. The top row shows structures of mono-M MXenes; the second row shows double-M solids solutions (SS) (green). The third-row shows ordered double-M MXenes (red). The fourth row shows an ordered di-vacancy structure, which has only been reported for the M_2C MXenes, making an $M_{1.33}C$ composition due to 0.33 atom % of vacancies in the M layers (pink) [53] Reproduced with permission © 2019, Springer

This review has its primary objective to review the fundamentals, structure and energetic aspects of Mxenes while providing a summary of various synthesis methods reported to date. The later sections of the review were dedicated to elucidating brighter prospects of MXenes in the energy storage field particularly for Li-ion battery (LIB), Li-Sulfur battery (LIS), and supercapacitors (SC).

2.Fundamentals of MXene

As of today, the MXene family includeTi_2C, V_2C, Fe_2C, Nb_2C, Mo_2C, Cr_2C, Ta_2C, Ti_3C_2, Hf_3C_2 Cr_3C_2, Nb_4C_3, , $Mo_{1.33}C$, Cr_2N, Ti_4N_3, Ti_3CN, , $(V_{0.5}, Cr_{0.5})_3C_2$, $(Ti_{0.5}\ Nb_{0.5})_2C$, Mo_2ScC_2, $Mo_2Ti_2C_3$, $(Nb_{0.8}Ti_{0.2})_4C_3$ and $(Nb_{0.8}Zr_{0.2})_4C_3$ [54,55]. According to n value in $M_{n+1}AX_n$ (n= 1 to 3), the atomic layers present in the MXene sheet

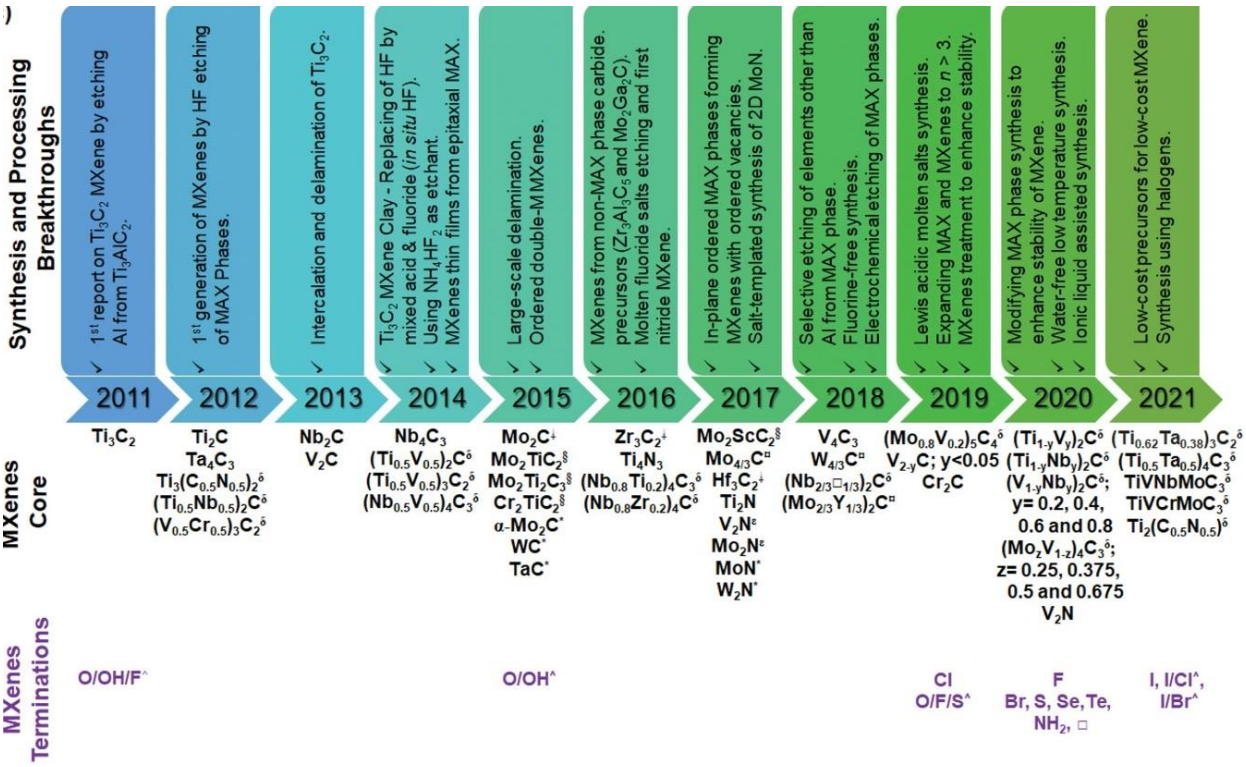

Figure 2. List of the main synthesis and processing breakthroughs over the first 10 years of MXenes' research, the new MXene core compositions discovered in that decade (surface termination abbreviation T_x is omitted in the chemical formula for simplicity) and progress in surface terminations control. [56] Reproduced with permission, © 2021, Wiley Online Library.

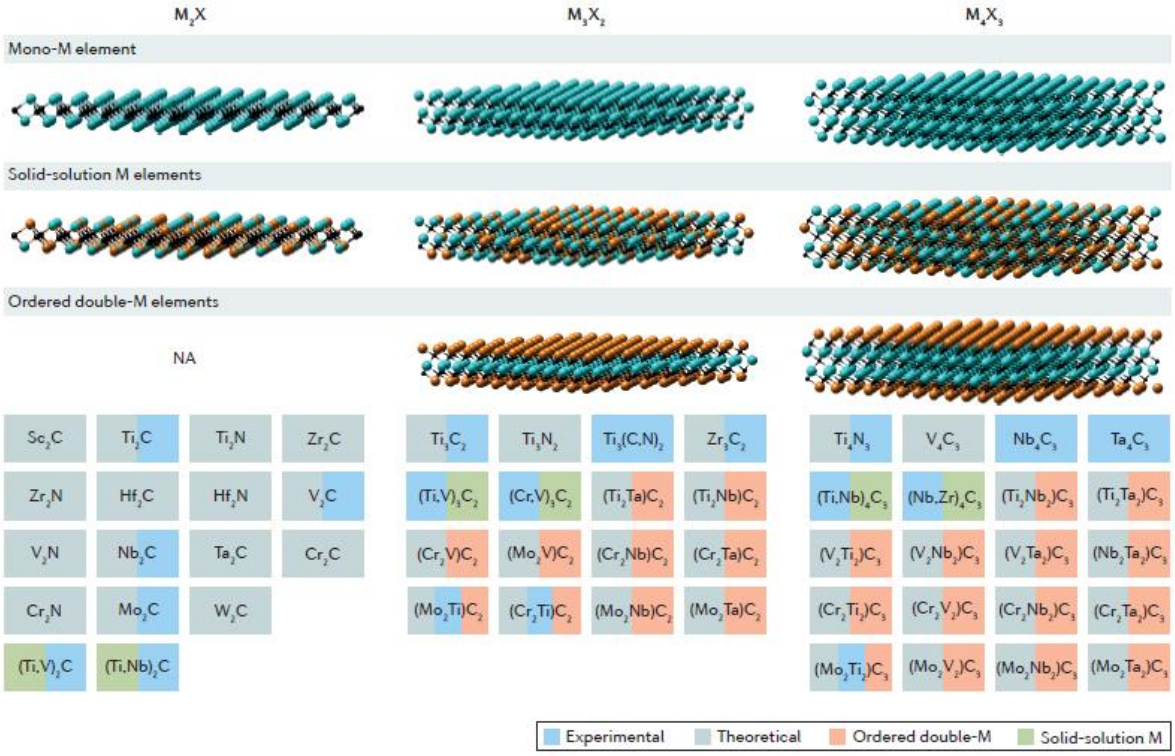

Figure 3. MXenes can have at least three different formulas: M2X, M3X2 and M4X3, where M is an early transition metal and X is carbon and/or nitrogen. They can be made in three different forms: mono-M elements (for example, Ti2C and Nb4C3);[57] Reproduced with permission, © 2017, Nature.

vary as 3, 5 and 7 respectively as shown in **Figure 3** while individual MXene layer thickness and lateral dimensions for all above cases are less than one nm and can reach up to 10 microns respectively [57].

2.1 Structure

Here of interest is to note that Mxene possesses several advantages for example (a) mechanical and chemical stability due to their ceramic nature, (b) they can exist in different forms such as single, few and multilayer's (c) it is possible to tune the number of valence electrons and relativistic spin-orbit coupling (SOC), (d) they can have controlled thickness of MXene monolayers which allows studying quantum confinement related phenomena; (e) different chemical groups attached at MXene surface offers functional surfaces and (f) Much like graphene, MXene exhibits massless Dirac dispersions in their band structure near the Fermi level [55].

Recently, density functional theory (DFT) calculations have proven the reliability of finding the chemical and physical properties of Mxenes. Using DFT calculations, the first structure of stacked Ti_3C_2 with –OH termination known as ML-MXene was predicted. The results obtained such as the c-lattice parameter obtained from the XRD

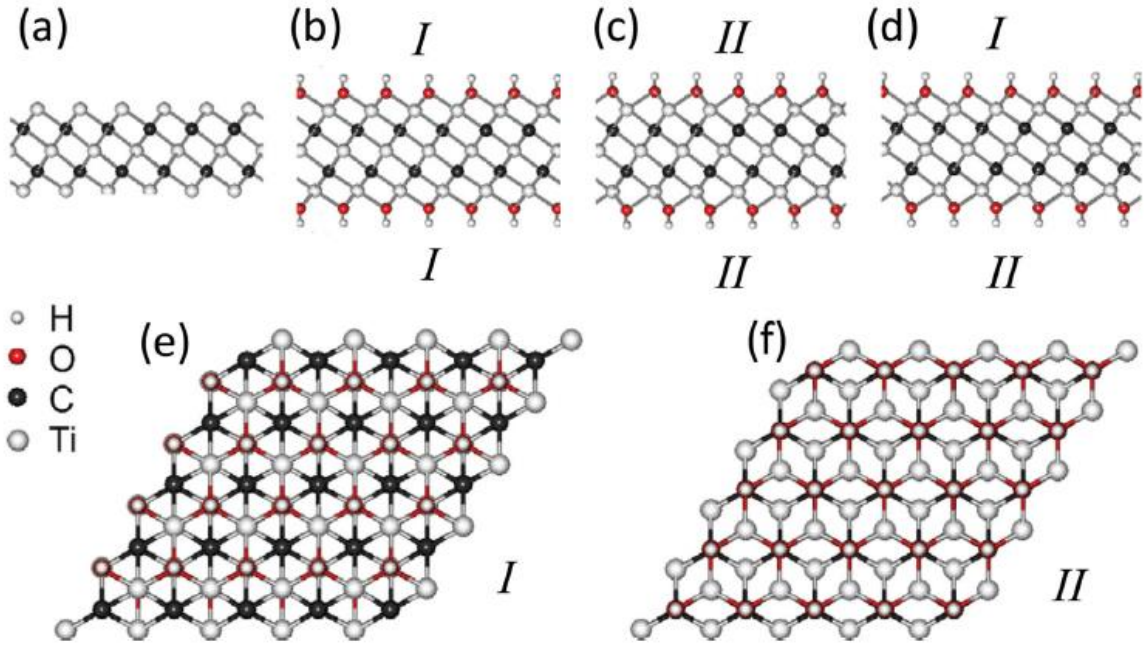

Figure 4. Configurations of functionalized MXenes with different arrangements of the surface atoms: side views of a) bare Ti_3C_2 b) I-$Ti_3C_2(OH)_2$ c) II- $Ti_3C_2(OH)_2$ and d) III- $Ti_3C_2(OH)_2$ e, f) top views of I- $Ti_3C_2(OH)_2$ and II- $Ti_3C_2(OH)_2$. [58] Reproduced with permission, © 2012, Elsevier.

characterization of fully hydroxylated MXene closely matched with the predictive simulations, even though a mixture of –OH and –F groups together could not be ruled out [59].

In the case incomplete or mixed –OH, -O, and –F termination situations become critical to understand, the presence of –O and –OH termination was confirmed with XPS [59,60]. Further complexity arises with the presence of water molecules in the interlayer space especially V_2C and Nb_2C MXene where the c-parameter value becomes much higher after etching [60]. Based on the DFT study, two distinct configurations I and II were predicted according to an energetically favourable orientation of T in Ti_3C_2T as shown in **Figure 4** [58,61]. In this configuration I, T terminals are situated above the hallowed site between three neighbouring carbon atoms, or in other words, T terminals point towards Ti(2) atoms on both sides of Ti_3C_2 layers [58]. On the other hand for II configuration, T terminals are above the C atoms on both sides of the Ti_3C_2 layers [58]. In the case of the hybrid system, both configurations I and II are present on the opposite sides of the sheet [61].

2.2. Synthesis methods

The precursor material used for MXene preparation is the MAX phase material which is the layered structure of carbides and nitrides with the general formula $M_{n+1}AX_n$ where n varies from 1 to 3, M stands for early transition metal (periodic table group 3-7), A is the 12-16 group element from the periodic table while X is the carbon or

nitrogen [62,63]. The MAX phase is generally prepared using less pressure calcination, for example, the Ti_3AlC_2 MAX phase is prepared using titanium, aluminium and graphite as a precursor calcinated under 20 MPa pressure. After four hours of calcination at 1400^0C, a single MAX phase can be obtained [64].

The conventional synthesis method for MXene is the wet chemical etching method where atomic layers are etched from a multilayer of MAX phase **(Figure 5a).** The MAX is socked in acid which eliminates the bond between transition metal element M and A element [65]. The bond between transition metal M and A in the MAX is stronger but due to acid socking, this bond is replaced with weaker hydrogen bonds such as –OH, -O or –F [7,8]. The HF acid is used for selective etching of A from MAX phase as shown in equation1 [54,66,67]:

$$M_{n+1}AX_n + 3HF \rightarrow AF_3 + 2/3H_2 + M_{n+1}X_n \quad (1)$$

The hydrophilicity present in the transition metal of $M_{n+1}X_n$ leads to fictionalizations of MXene with -OH, -O, -F groups are shown by the equation 2 and 3 [54,66]:

$$M_{n+1}X_n + 2H_2O \rightarrow M_{n+1}X_n(OH)_2 + H_2 \quad (2)$$

$$M_{n+1}X_n + 2F \rightarrow M_{n+1}XnF_2 + H_2 \quad (3)$$

Since etching and exfoliation processes do not occur simultaneously in the case of the HF etching method, hence further delamination steps become necessary as shown in **Figure 5b.** To obtain a single or few-layered Mxene delamination step performed, intercalation with a solution like DMSO or isopropyl alcohol and simple shaking/sonication can delaminate multilayered MXene [68,69]. The experimental results demonstrated that the MXenes prepared via HF etching possess excellent electronic conductivity and showed lower atomic defects. Thus, the HF treatment process is useful only for carbon-based MXene but not for the nitride-based MAX [65].

The etchant used for this reaction is HF, an acid material that is toxic and dangerous to the environment hence a replacement of HF is desirable. For safer side mixture of hydrochloric acid and fluoride salts such as LiF is used for the preparation of MXene where the reaction between HCl and fluoride salts result in HF formation, which indicates the formation of fluoride during this reaction [70,71]. The time required for exfoliation, in this case, is more than the time required for HF etching. In the case of HCl and fluoride salt as an etchant, a separate delamination process is not required due to the metal ions like Li^+ present in the solution increasing interlayer spacing [70]. The etching and delamination process decides the properties of MXene such as its crystallinity, quality of flakes, atomic defects, fictionalizations of the surface and thickness [72,73].

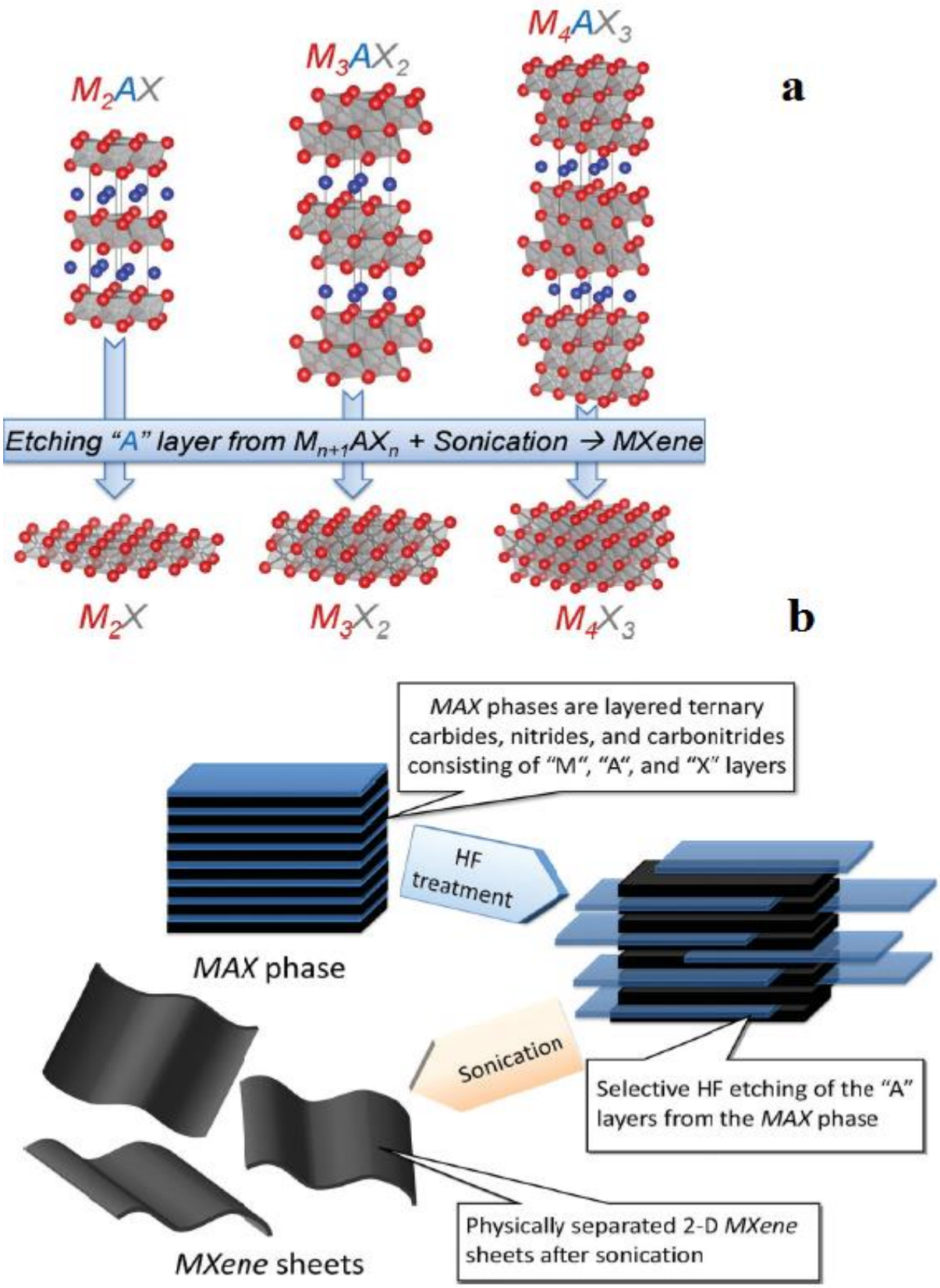

Figure 5 a. Structure of MAX phases and the corresponding MXenes. [74] b. Schematic describing the synthesis process of MXenes from MAX phases. [8] Reproduced with permission, © 2012, Americal Chemical Society.

The problem remains unsolved about the use of (HCl + LiF) because of the in-situ formation of HF [75]. This problem can be solved by developing novel methods to bypass the use of HF acid or HF based products using methods discussed next:

2.2.1. Chemical Vapor Deposition

The chemical vapour deposition method uses a bottom-up approach opposite to the approach used in the chemical etching method and hence it is possible to synthesise rich and large quantities of MXenes along with controlled thickness [76]. In 2015 for the first time, Xu et al [77] reported a chemical vapour deposition method for the synthesis of MXene where methane was used as a source of carbon and copper slitting on the Mo foil at a temperature more than 1085^0C. In this method, active mass was deposited on the substrate in terms of thin-film, from a vapour phase generated from the precursor. At the high-temperature, copper film melts leading to the formation of Cu-Mo alloy at the liquid Mo/Cu interface. Simultaneously, the carbon atom from decomposed methane and Mo atom from the interface diffuses on the surface of the copper liquid and form Mo_2C [78]. Xu et al. [77] also demonstrated that the change in experimental conditions can affect the size and thickness of the Mo_2C crystal for example with increasing growth temperature, nucleation density increases while increasing growth time increases the lateral size. The MXene material obtained from the experimentation was a few nanometers thick and the lateral size was more than 10 μm. Also, the material was free from defects and its conductivity was stable even in materials that came in contact with air [78]. Geng et al. [79] reported a molten copper-catalyzed CVD method for the synthesis of Mo_2C crystal on *in-situ* grown graphene film and high-quality and uniform Mo_2C film in the centimetre range was successfully grown on graphene using a Mo–Cu alloy catalyst.

Apart from Mo-MXene other two-directional ultrathin transition carbides such as TaC and WC crystals can be synthesized using a CVD method [80]. The MXene obtained from the CVD method with a much lower density of defects and disorder as well as a lower concentration of impurity [78].

2.2.2. Urea Glass Route

In 2015, Ma et al. [81] reported HF free synthesis method for carbide and nitride-based MXenes where Mo_2C and Mo_2N MXene were synthesized using urea glass route from $MoCl_5$ precursor. In this method, precursor $MoCl_5$ was added in ethanol to form Mo-orthoesters. Next, urea was added to the solution and stirred till it becomes completely soluble. The gel-like precursor obtained was placed in the crucible and heated at 800^0C under N_2 gas flow for 3 hrs. Finally, silvery black powder was obtained after the calcination. The XRD characterization demonstrated the synthesis of high purity Mo-based carbide and nitride, with no other impurities like MoO_x or Mo metal present in the prepared sample. The average size of obtained Mo_2C and Mo_2N was 11 nm and 16 nm respectively [81].

2.2.3 Molten Salt Etching

In 2016, the molten salt etching method was used for the first time to synthesise MXene materials by Gogotsi's group at Drexel. Until this synthesis method was realised, nitride-based MXenes could not be produced. The method used for the synthesis of carbide-based MXene was unable to apply for nitride-based MXene production due to various reasons. For example, the calculated cohesive energy for $Ti_{n+1}N_n$ is less than the $Ti_{n+1}C_n$ while $Ti_{n+1}N_n$ has higher formation energy than the $Ti_{n+1}AlN_n$ MAX phase compared to titanium carbide. The lower cohesive energy means the lower stability of the $Ti_{n+1}N_n$ while more formation energy leads to the stronger bond of the Al atom in $Ti_{n+1}AlN_n$ hence higher energy is needed for extracting the Al layer from $Ti_{n+1}AlN_n$ [82]. Another limitation of the HF etching may be ascribed to the lower stability of $Ti_{n+1}N_n$ and during the etching process, $Ti_{n+1}N_n$ can dissolve in the HF solution [74]. To etch Al from Ti_3AlN_2 MAX, molten fluoride salt was used at a temperature of 550^0C in an Ar gas environment. This reaction forms different Al-containing fluoride phases except for the Ti-fluoride which clears selectivity of etching. The fluoride was dissolved using dilute H_2SO_4 solution which washed Al-containing fluoride phases using DI water. The XRD results demonstrated all fluoride salt was removed and what was left was the $Ti_4N_3T_x$ and unetched Ti_4AlN_3. Further, the powder was treated with tetrabutylammonium hydroxide (TBAOH) and washed with DI water. Finally, after sonication, smaller unlayered $Ti_4N_3T_x$ flakes were collected **(Figure 6a)** [83]. The material possessed more atomic defects than MXene obtained from HF-etching, which affects the breaking strength of the material.

2.2.4 Ultra-Violet Light-Induced Etching

In 2020, Mei et al. [84] introduced an ultra-violet (UV) light etching method for the synthesis of Mxenes from Mo_2Ga_2C. The Mo_2Ga_2C is a promising UV absorbing material with increased absorption from infrared to UV region and such UV responsive property was used for selective etching of double-layered Ga atoms from Mo_2Ga_2C **(Figure 6b)** [85]. In this method, selective etching of weakly bonded Ga atom was conducted using a UV light for several hours and by using milder H_3PO_4 solution. The Mo_2CT_x MXene obtained from the method demonstrated that the 2D sheets were produced in a much shorter time [84].

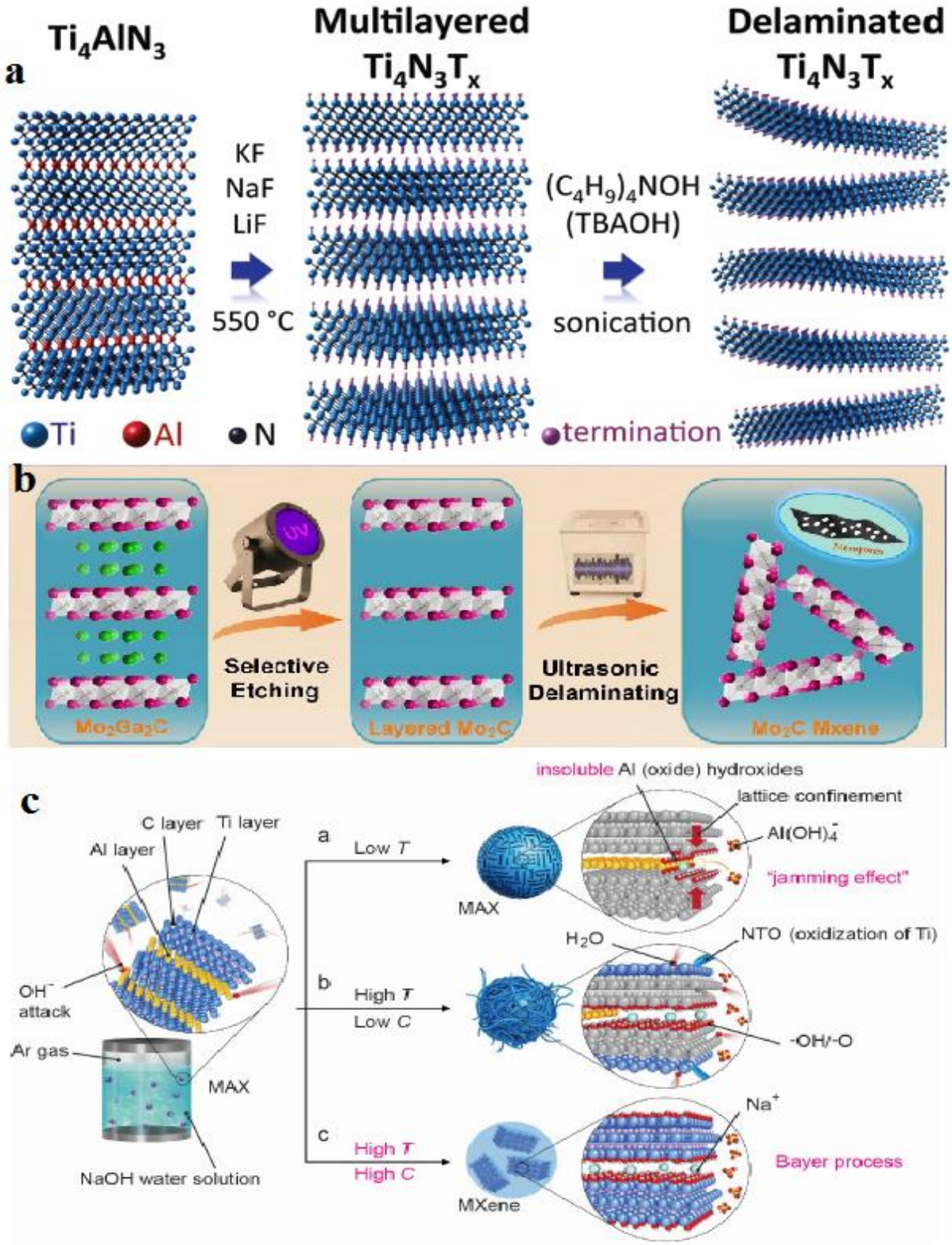

Figure 6 a. Schematic illustration of molten salt treatment [71] **b.** Schematic illustration of UV-induced selective etching synthesis of two-dimensional (2D) mesoporous Mo_2C [72] **c.** Schematic of the reaction for a hydrothermal method for MXene preparation [74] Reproduced with permission, © 2014, American Chemical Society.

2.2.5 Hydrothermal Method

Hydrothermal process is the one of the simple and easy one step process used in synthesis of nanostructured materials for various applications [35]. In 2018, Li et al. reported HF-free synthesis of $Ti_3C_2T_x$ via alkali treatment. In this method, pristine Ti_3AlC_2 was treated with NaOH water solution with the hydrothermal method, where hydroxide ions ($OH^{-)}$ attacked the Al layer in the Ti_3AlC_2 MAX phase leading to oxidation of Al atoms to form $Al(OH)_3$ and their dehydrated oxide hydroxide AlO(OH). The lattice confinement generated from the Ti layer prevents the conversion of these insoluble compounds to dissolvable $Al(OH)_4^-$ by reacting with OH^-, called as jamming effect block further MXene formation **(Figure 6c)** [86]. The problem was overcome by following the Bayer process where the application of a series of temperatures and concentration of NaOH water solution under Ar treatment to alleviate sample oxidation. Using this method fluoride-free multilayer Ti_3C_2 MXene was prepared with 92% purity where 27.5 M NaOH was used as an alkali solution at 270^0C hydrothermal temperature [86].

2.2.6 Electrochemical Synthesis

The binary aqueous electrolyte was first used in 2018 for delamination of Ti_3C_2 without the use of HF. Yang et al. [87] first demonstrated anodic corrosion of Ti_3AlC_2 in binary aqueous solution for the synthesis of MXene. In this process, chloride enabled rapid ionic Al etching and breaks the Ti-Al bond. The aluminium hydroxide was subsequently used for intercalation where it opens the edges of the etched anode resulting in etching under the surface. At ambient temperature and within a short period, anode Ti_3AlC_2 was etched completely and more than 90% of the material was single or double-layered having an average lateral size of more than what's achieved in conventional HF-etching. Also, fluoride terminal groups were completely absent in the $Ti_3C_2T_x$ MXene. The electrical conductivity of the Ti_3C_2 MXene was the same as the HF-etching method [87]. Electrochemical etching is the most promising approach among all other etching methods, up to 60% of the bulk material can be transformed into $Ti_3C_2T_x$ [87]. Table 1 illustrates various parameters of the synthesis methods for MXene.

Table 1 Comparison of parameters used for various synthesis methods for MXene preparation also obtained products image and specialities of the used method.

Synthesis Techniques	**Applicable Precursor MAX/obtained MXene**	**Etching agent/ sources**	**Sample SEM/TEM/ Optical images**	**Properties. Terminals, size of flakes**	**Specialities of method**	**Ref.**

HF etching	All carbide MAX/MXene	HF/NH_4HF_2	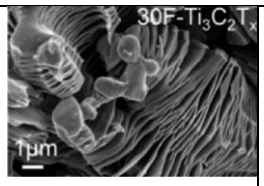	1) Small flake size, abundant defects. 2) Accordion like structure with terminals like –O, -OH, -F	Merits: High selectivity and acceptable yields Demerits: Abundant defects and hazardous method	[88] Reproduced with permission, © 2017, American Chemical Society
Fluoride-based salt etching	$Ti_3AlC_2/(Ti_3C_2)$ $Mo_2GaC/(Mo_2C)$ $Ti_2AlC/(Ti_2C)$	LiF/NaF/KF +HCl or NH_4HF_2	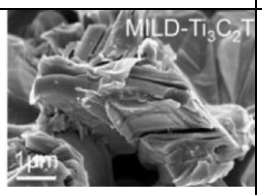	Large internal spacing with high –O termination 2) Large flake size with few defects	Merits: Low defects; less hazardous; large flake size Demerits: higher etching temperature and longer time	[88] Reproduced with permission, © 2017, American Chemical Society
Molten salts etching	$Ti_2AlC/(Ti_2C)$ $Ti_4AlN_3/(Ti_4N_3)$	LiF + NaF + KF	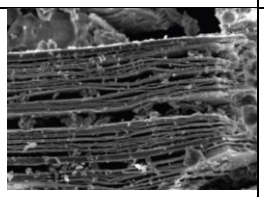	1) Accordion-like structure with TiO2 phase 2) Small flake size with many vacancies and defects	Merits: synthesize MXene, which is low stability in HF solution Demerits: high temperature; low crystallinity of Mxene	[83] Reproduced with permission, © 2016, Royal Society of Chemistry
Hydrothermal method	$Ti_3AlC_2/(Ti_3C_2)$	NaOH	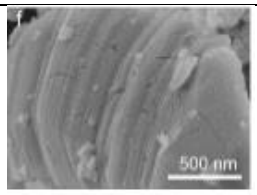	More –OH and –O terminals Fluoride terminal completely absent	Merits: Easy synthesis	[86] Reproduced with permission, © 2018, Wiley - VCH Verlag GmbH

Chemical Vapour deposition	Not Applicable/Mo_2C	Cu foil/Methane	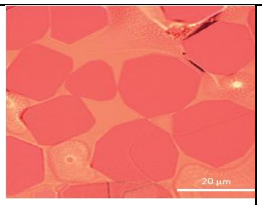	Defect-free MXene with larger lateral size obtained	Merits: High conductivity, Controlled thickness Demerits: Not valid for all MXene	[78] Reproduced with permission, © 2015, Nature Publishing Group
Urea Glass route	Not Applicable/Mo_2C/Mo_2N	$MoCl_5$+Ethanol/Urea	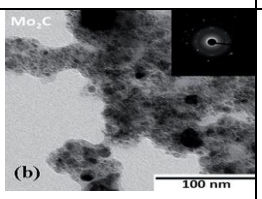	Small Particle size 11 and 16 nm For Mo_2C and Mo_2N resp.	Merits: High purity Demerits: Only applicable for Mo-MXene	[81] Reproduced with permission, © 2015, Royal Society of Chemistry
UV light etching	Mo_2GaC/(Mo_2C)	H_3PO_4	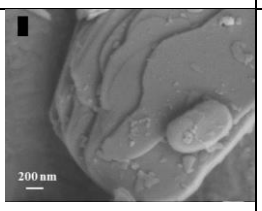	1.2D sheet without contaminants 2. –F terminal absent completely	Merits: Shorter etching time Demerit: Only applicable for UV responsive material	[84] Reproduced with permission, © 2020, Elsevier B.V.
Electrochemical Etching	Ti_3AlC_2/(Ti_3C_2)	NH_4Cl/ Tetramethyl ammonium hydroxide (TMAOH)	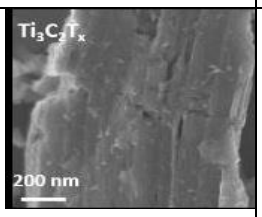	1.-OH and –O Terminal group 2. size 18.6 um	Merits: Most promising method, 60% material transformed Good electrical conductivity	[87] Reproduced with permission, © 2018, Wiley-VCH Verlag GmbH & Co. KGaA

3. Fundamental Properties

3.1 Chemical properties

To understand the chemical composition and stoichiometric ratio, analysis of the local chemical environment is necessary. Naguib et al. [89] reported that $Ti_3C_2T_x$ oxidizes in environments like air, CO_2 or pressurized water where anatase TiO_2 (TiO_2-C hybrid structure) is embedded in an amorphous C sheet generated after oxidation of $Ti_3C_2T_x$. Similarly, other hybrids like Nb_2O_5/C were produced from Nb_2C after oxidation. Also, the in-situ oxidation process of MXene was studied using the TEM characterization technique coupled with Raman spectroscopy. It was considered that during flash oxidation, the top and bottom titanium layer oxidized to form thin anatase nanoparticles while during slow oxidation they transformed to planer nanocrystalline rutile. Results demonstrated two different TiO_2 phases exhibited according to controlling time, temperature and heating rate [90]. Li et al. [91] discovered that $Ti_3C_2T_x$ could react with O_2 to form TiO_2 either in any of two forms (anatase or rutile). At 200^0C in an oxygen environment, part of the MXene layers oxidized to anatase nano-crystals evenly distributed on 2D later of Ti_3C_2 while at 1000^0C MXene layer completely oxidized the anatase phase transformed to rutile in an oxygen environment. In contrast to the TiO_2-C hybrid structure, the anatase nano-crystal distribute evenly on the 2D Ti_3C_2 layer. The difference in the chemical structure stems from a longer reaction time of approximately 40 min while in the case of TiO_2-C, flash oxidation (<5 sec) is likely. Similar results are observed for Ti_2CT_x by Li et al. [92] where with heat treatment, anatase TiO_2 formed before transforming to rutile TiO_2 at high temperature.

3.2 Structural Properties

The Model structure of the MXene ($M_{n+1}X_n$) material was prepared by removing the A layer from the MAX phase ($M_{n+1}AX_n$). MXene demonstrated hexagonal lattice originating from the hexagonal symmetry of the MAX phase. The 2D M_2X MXene possesses a hexagonal unit cell with trilayer sheet carbon/nitrogen (X) sandwiched between two transition metal layers [55,93,94]. The transition metal atoms in the MXene can create six chemical bonds with neighbouring X atoms and other groups on the surface such as –OH, -O, or –F [95]. Two types of hallow sites are present on the surface of M_2X such as hallow site A under which no X atom is present between the TM layer and the hallowed site while in other cases hallow site B where X atom is present a lower panel. Hence, based on this information for the M_2X system, four configurations are possible based on the relative position of the terminal groups linked to the surface of TM [55]. The Model I- two T_x positioned on the top of the two TMs; Model II- two T_x on the top of hallow site A; Model III - one of the T_x on the top of hallow site A and other is on the top of hallow site B; Model IV- two functional groups on the top of hallow site B, Model II and IV respectively [55, 96] [95].

For stability study, these four configurations were considered for each T_x with a fully relaxed atomic position. Generally, functionalized MXene Model-I represents poor stable structure compared to the other 3 models in many studies and during structure optimization this Model I transformed into Model II to IV [55]. The stability of models mainly decides the possible ionic states for TM on the surface of MXene. The availability of sufficient TM electrons to X and attached functional groups can decide more stability of Model II otherwise Model III or model IV is a more stable configuration [95]. The formation energy evaluation can give the stability information of functionalized MXene. The First-principle calculations show that when MXene surface becomes functionalized, they can gain more negative formation energy leading to the formation of a strong bond between TM atom and functional groups and it encourages the synthesis of MXene with specific surface functionalization [95]. Also, it has been theoretically examined that functionalized MXenes are thermodynamically more stable than non-functionalized MXenes [95,97]. In some MXenes, it has been theoretically found that at a particular chemical potential, surfaces are fully functionalized. The MXene with full surface functionalization are locally stable proven by the Phonon frequency analysis [95,98–100].

In all practical situations, MXene comes with surface functional groups such as -F, -OH and -O from the MAX precursor only after exfoliation. The stability of hydroxyl and/or oxygen surface functional groups (T_x) terminated MXene are higher compared to –F terminated MXene because with water treatment/rising –F termination can be replaced with -OH groups [55]. Also, high-temperature treatment and/or metal adsorption process can convert -OH group into -O termination [101,102]. Finally, the –O terminated MXene can be transformed to bare MXene if brought in contact with Mg, Ca, Al or other metals [103].

3.3 Electronic Properties

The electronic properties of MXene play a vital role in various applications and similar to the MAX phase pristine MXene possesses metallic characteristics. Though recent studies have made many attempts to enhance electronic conductivity, the first time discovered and most studied MXene, $Ti_3C_2T_x$ is still reported to be most conductive [104][105]. However, some types of MXenes upon surface functionalization transfers from metallic to semiconducting states. Based on theoretical studies, MXene is categorized into two groups according to their spin-orbital coupling; topologically trivial [106] and non-trivial [107–111], while based on the strength of relativistic SOC it can be categorized into metal, semi-metal and semiconductor [106].

3.3.1. Topological Trivial metal and semiconductors

Even though most MXenes are metallic, Ti_2CO_2, Zr_2CO_2, Hf_2CO_2, Sc_2CT_x (T_x- F, OH, O and x=2) become semiconductive after surface functionalization. The general gradient approximation (GGA) revealed energy gap of 0.24 eV, 0.88eV, 1.0 eV for Ti_2CO_2, Zr_2CO_2 and Hf_2CO_2 respectively while for Sc_2CT_2 for T - F, OH, O were

estimated to be 1.03 eV, 0.45 eV and 1.8 eV respectively [106]. Except for $Sc_2C(OH)_2$, all above semiconductors have indirect bandgap [96,106]. Other early transition metals like Ti, Hf and Zr are present in the same periodic group 4, hence they possess the same number of valence electrons and corresponding MXene after functionalization behaves similarly as metallic to semiconductor [96,106]. Also, it has been predicted that the similar oxidation state of the -F and -OH functional group which accepts only one electron from the surface, can similarly affect the electronic structure of MXene. In contrast to -F and -OH, -O functional group demands two electrons from the surface hence, it behaves differently [106].

To understand the transformation of MXene from metallic to semiconductor, an electronic structure study of MXene with and without functionalization is necessary [106]. The pristine M_2X exhibited metallic behaviour having Fermi energy level locating at d band of TM (M) demonstrated by molecular calculations [96]. The p band of the C/N (X) present in most of MXene is below the d band of transition metal M with a small bandgap. Due to the functionalization of -F, -OH or -O, a new type of band forms below the Fermi energy [96]. This occurs due to the hybridization of d orbital's from transition metal M and p orbital's from -F or -O. Transformation of metallic to semiconductor in case of Ti_2CO_2, Zr_2CO_2, Hf_2CO_2 and Sc_2CT_2 (T- OH, F or O) occurs due to Fermi energy shifts to the centre of the d band of transition metal and p band of carbon/nitrogen [55,112]. Ti_2CF_2 remain metallic because of no shift in Fermi energy. **Figure 7** demonstrate the projected DOS and band structure for Ti_2C, Ti_2CO_2 and Ti_2CF_2 [96,106].

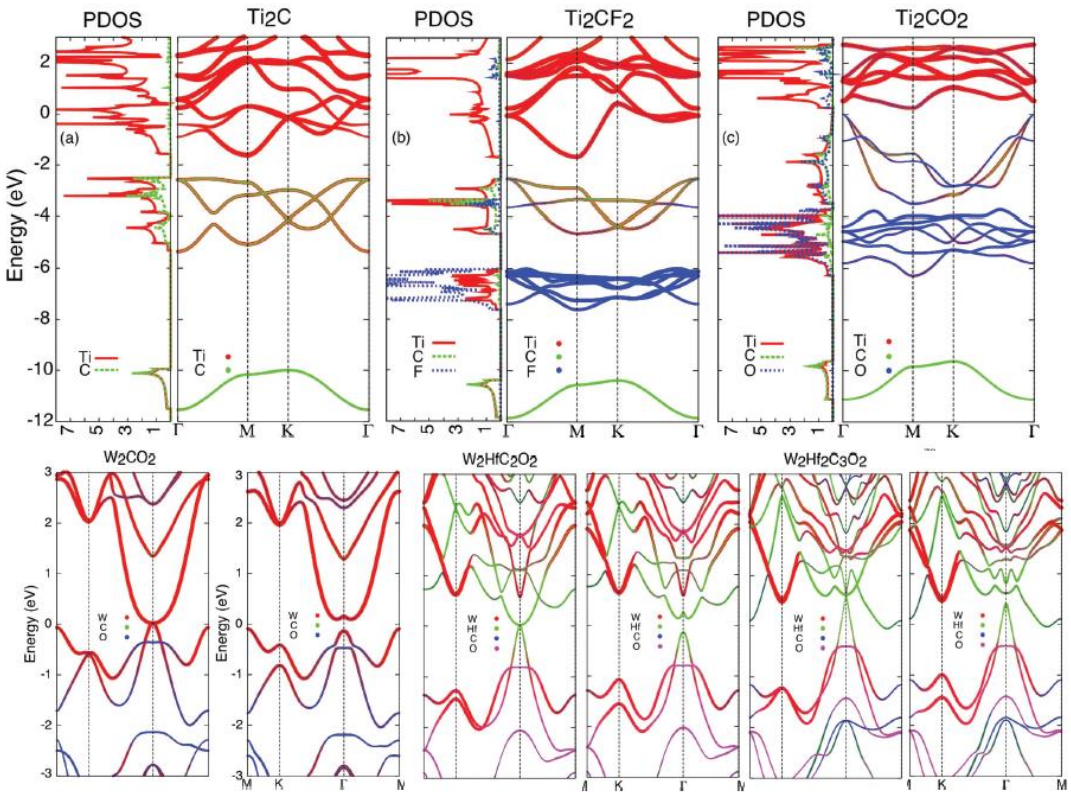

Figure 7 a. PDOS and projected band structures for Ti_2CT_x [93]. Reproduced with permission, © 2014, Americal Chemical Society.

3.3.2. *Topologically Non-Trivial semimetals and semiconductor*

In the case of 4d and 5d heavy transition metal-based MXene, the electronic structure gets influenced by the relativistic SOC effect [96,110,111]. When the SOC effect is not considered, the W_2CO_2, Mo_2CO_2 and M′M″CO_2 (M′ = W and Mo; M″= Ti, W, Zr) are semimetals because only at point Γ, topmost valence band touches the lowest conduction band, around which valence and conduction band both are parabolic [96,110,111]. The band near Fermi energy originates from d orbital of M, M′ and M″ revealed by the projected band structure [110,111]. Considering spin-orbital coupling bandgap for MXene opens at Γ point due to degeneracy of the topmost valence band and lowest conduction band at Fermi level energy [96]. Consequently W_2CO_2, Mo_2CO_2 and M′M″CO_2 transformed into a semiconductor state with indirect bandgap and induced bandgap increased as the SOC effect increases [96]. The band gaps are 0.194 eV (0.472 eV) for W_2CO_2 and 0.285 eV (0.401 eV) for $W_2HfC_2O_2$ within GGA. However similar features have not been observed for $M'_2M''_2C_3O_2$ (M′ = W and M″= Ti, Zr, Hf) and these systems remain semimetal even after applying SOC [55].

3.4 Mechanical Properties

The surface functional groups may drastically change the mechanical properties of MXenes. Zha et al. [113] performed density functional theory calculations to investigate the mechanical properties of carbide MXenes. The research group analyzed that the –O functionalized MXenes have smaller lattice parameters and stronger mechanical strength compared to the -F or -OH functionalized MXene. W_2CO_2 showed higher mechanical strength while Sc_2CO_2 showed the smallest interlayer spacing [113]. Bai et al. [114] reported the influence of surface termination of Ti_2CT_2 and $Ti_3C_3T_2$ (T = O, OH and F) to investigate the mechanical properties using DFT and found stronger interaction between Ti and -O than other surface terminal groups -F and -OH in case of Ti_2CT_2 and $Ti_3C_3T_2$ MXene. The O-terminated MXene showed a very high stiffness than the -OH terminated and –F terminated MXene, which was attributed to the strong bond between Ti-O [111]. Magnuson et al. [115] studied chemical bonding in $Ti_{n+1}C_nT_x$ (n =1,2) using surface sensitive XPS. The stacked nanosheet with a variety of thicknesses changed the band structure, analyzed in connection with known hybridization region TiC and TiO_2 which influenced the elastic properties of MXene. The result demonstrated that the surface functional groups withdraw charges from the Ti-C bond and weaken them. The T-C bond length was larger for Ti_2CT_x than $Ti_3C_2T_x$ which directly affects the elastic properties of the MXene [115].

Chakraborty et al. [116] reported the effect of alloying on the mechanical properties of MXenes such as their elastic properties, critical strain and stiffness. They proved using the first-principle calculations that doping of B

and V at Ti and C sites of Ti_2C can improve in-plane stiffness, Young's modulus and critical strain. The oxygen passivation of B doped Ti_2C makes a reasonable change in critical strain along with superior elastic properties. Yorulmaz et al. [117] reported that as the mass of the transition metal M increases, carbide MXene becomes stiffer but the same is not true with the nitride MXenes. Most of the carbide-based MXene are considered mechanically stable; the same case is not true for the nitride-based MXene. Single flake MXene containing oxygen was seen as unstable in the water in an open environment while they were stable in water once oxygen was removed [118,119].

3.5 Magnetic properties

The strong covalent bonding between transition metal M, C/N elements and T_x results in a majority of MXenes being nonmagnetic, especially at the ground state becoming revealed by the spin-polarized DFT [96,106]. By applying strain, the band gap can be engineered which was seen to cause the release of *d* electrons while bringing magnetism [96,120]. On the other side, some pristine MXene exhibits intrinsic magnetism e.g. pristine Ti_2C and Ti_2N are nearly half-metallic ferromagnetic with a magnetic moment of 1.91 and 1.0 μB per formula of the unit [55,121]. With the continuous increase in the biaxial strain, nearly half-metal ferromagnetic monolayer Ti_2C transformed into perfect half metal, spin gapless semiconductor and then metal. While in the case of the monolayer, Ti_2N remains nearly half-metallic even after applying biaxial strain [96,121].

A monolayer of V_2C and V_2N is antiferromagnetic and non-magnetic metals respectively but a large amount of magnetic moment can be induced by applying biaxial and compressive strain [96,121] Also, functionalization of V_2C of F or OH can convert into a small gap antiferromagnetic semiconductor [96,122].

In the case of Cr-MXene, Cr_2C and Cr_2N are both magnetic due to the presence of *d* electrons Cr. Cr_2C is half-metallic ferromagnetic while functionalization transform into antiferromagnetic semiconductor [96,123]. After F, O, or OH surface functionalization of Cr_2N, half-metallic behaviour appeared [124]. This characteristic is vital because the synthesis of pristine half-metallic MXene such as Cr_2C using the etching technique is very difficult. Also, the magnetic and non-magnetic state energy difference is so large for Cr-MXene that these systems can retain magnetism nearly at room temperature [125]. Hence MXenes is considered a strong contender for spintronic applications. It is possible to induce magnetism in nonmagnetic MXenes for example by doping Ti, V, Cr or Mn in Sc_2CT_2. It was shown that manganese and chromium are promising dopants to transfer non-magnetic Sc_2CT_2 into magnetic version [96,126].

Recently, ordered double metal carbide, $Cr_2M''C_2T_2$ MXene (M″ = Ti and V) materials magnetic properties have been studied and it was found that depending on M″ and T elements $Cr_2M''C_2T_2$ can be antiferromagnetic, ferromagnetic or non-magnetic also either metallic or semiconductor [96,127]. For example, $Cr_2TiC_2O_2$ is non-magnetic, $Cr_2TiC_2F_2$, $Cr_2TiC_2(OH)_2$ are antiferromagnetic and $Cr_2VC_2O_2$, $Cr_2VC_2(OH)_2$, $Cr_2VC_2F_2$ are

ferromagnetic. The Curie temperature of 618.36^{0}C and 695.65^{0}C were estimated for $Cr_2VC_2(OH)_2$, $Cr_2VC_2F_2$ respectively.

4. Progress in MXene family

In 2012, other new members e. g. Ti_2CTx, $(Ti, Nb)_2CTx$ and $(V, Cr)_3C_2Tx$ were reported [7,57]. Later on, different structured MXene members such as small flake, delaminated single layer, double M member, and ordered divacancies were also discovered [128]. Even though the MXene family explored at a large scale $Ti_3C_2T_x$ is considered as a base for further investigation of the MXene family [57,129].

To date, more than 30 species of MXenes have been obtained experimentally while more than 70 MAX phases are available. Also using computational methods dozens more have been explored while some expected to form solid solutions like $(Ti, Nb)CT_x$. Some double M elements ordered MXene have also evolved where some form an atomic sandwich of transition metal planes (2 > n) e. g. Mo_2TiC_2Tx or (n=1) in-plane ordered structure like $(Mo_{2/3}Y_{1/3})CT_x$. Ordered divacancy has also been reported for M_2C MXene e.g. $Mo_{1.33}C$ due to 3 atom percentage vacancy at the M layer [130].

Among existing MXene, Ti-MXene has been widely explored and acquired in maturity in successful use in various applications [131,132]. The synthesis of Ti-MXene heavily depends on HF acid which raises safety concerns and waste management. Also, control over properties becomes difficult due to a lack of control over the termination group [133–135]. In that context, heavy research is going on to develop new MXene systems which possess characteristics to solve current challenges and improve the Mxene functionalities [76]. Apart from Ti-MXene, new MXene systems with early TMs like Mo, Cr, V, Nb, Hf and Ta have attracted attention due to their excellent characteristics over Ti-MXene [130]. For example, Mo base MXene stability is much higher than the Ti-MXene also it possesses fewer termination groups than Ti-MXene due to less contribution of electrons to the termination group [136]. The case of V-based MXene has more Li^+ storage capacity than the Ti-MXene while Nb-MXene has superior biocompatibility and biodegradability compared to Ti-MXene [137,138].

4.1 Mo-MXene

The Mo-MXene is a more stable material than the $Ti_3C_2T_x$ and is also considered a unique MXene system in the MXene family [139]. Mo-MXene is the only phase of the Mxene family that can be synthesized using the CVD synthetic method. Mo-MXene can also be synthesized by selective etching of the MAX phase and it has become possible due to the discovery of the Mo_2Ga_2C MAX phase in 2015 [140]. In Mo_2Ga_2C MAX phase possess two A layer (Ga in this case) different from other MAX phases which open a new window for Mo-MXene. In 2016 Halim et al. [141] reported Mo_2CT_x MXene by selective etching of Ga from Mo_2Ga_2C using HF and HF-based products. The etching time required for Mo_2Ga_2C was much longer than the time required for Ti-MXene which is

approximately 157 hrs. In Mo_2CT_x as temperature decreases from 300 K to 10 K, the resistivity increases by an order of magnitude suggesting semiconductor behaviour in contrast to metallic behaviour for $Ti_3C_2T_x$. Further, to reduce etching time and avoid toxic HF acid use Mai et al. [84] reported UV induced selective etching method to fabricate fluorine-free mesoporous Mo_2C MXene. The material they obtained demonstrated that it is possible to obtain Mo_2CTx within a short period of etching (3 to 5 hrs) as compared to acidic etching using this method.

As top-down approaches like selective etching methods suffer from issues like thickness control, bottom-up approaches such as the chemical vapour deposition methods grow fast to synthesise MXene with controlled thickness and chemical formula [141,142]. Using chemical vapour deposition (CVD) methods, other 2D materials such as graphene [143], transition metal dichalcogenides like $MoSe_2$ [144], MoS_2 [145], WS_2 [146] and boron nitride [147] have been synthesized and this synthetic technology achieved maturity for this material but MXene synthesis using CVD method is in early-stage and only the Mo-MXene are synthesized using this method. Geng et al. [148] reported molten Cu catalyzed CVD methods for one-step direct synthesis of 2D Mo_2C on graphene which demonstrated well faceted large size single crystal having low defect density. Recently, liquid metal substrates were used for the synthesis of two-dimensional materials. Sun et al. [149] reported liquid metal Au as a substrate for the synthesis of two dimensional Mo_2C and Mo_2C-graphene heterostructures using CVD method. The parameters like quantity of hydrogen and hydrogen/carbon ratio effected the quality growth of Mo_2C and graphene.

Another MXene grown using the CVD method is the Mo_2N. Joshi et al. [142] reported a two-stage approach phase transforming 2D oxides for the synthesis of MXene of nitride. Using the hot filament CVD method initially MoO_3 was prepared on FTO glass and subsequently annealing in ammonia atmosphere it was transformed to Mo_2N. Nitridation and exfoliation of MoS_2 can also give better quality Mo_2N MXene. Sun et al. reported Na_2CO_3 assisted nitridation and exfoliation of natural 2H-MoS_2 in NH_3 environment at 700-800^{0}C. The presence of Na_2CO_3 and MoS_2 in NH_3 topochemical transformation started leading to the formation of Mo_2N. This synthesis process shortens nitridation of conventional MoS_2 time up to 2 hrs, in contrast to the absence of Na_2CO_3 requires 40 hours [150]. The chemical vapour deposition method is free from toxic precursors as required in the chemical etching method and it is possible to get without T_x groups (O-, -OH, -F etc.) [151] [142,148,152]. Also, sources used during nitridation can be controlled easily resulting in controlled synthesis of MXene. From the above discussion, it is clear that a new window for other MXene nitrides synthesis can be realised using advanced nitridation processes.

The defective Mo-MXene has also recently attracted attention [153]. It was an unexpected result obtained during the etching of $(Mo_{2/3}Sc_{1/3})_2AlC$. During the etching process along with the Al layer Sc layer also got etched which

resulted in the formation of $Mo_{1.33}CT_x$ with ordered vacancy. The time required for etching during the formation of defective Mo-MXene was shorter than that of Mo_2CT_x [154].

4.2 V-MXene

In 2012, V-containing MXene ($(V_{0.5}Cr_{0.5})_3C_2T_x$) was synthesized for the first time and subsequently V-base and V-containing MXenes emerged. The surface layers in V-MXene are potentially responsible for capacitance, especially pseudocapacitive behaviour. The V_2CT_x exhibit higher theoretical specific capacitance than most popular Ti-MXene $Ti_3C_2T_x$ and hence a lot of attention was made to the V-MXenes for their potential applications in energy storage technology.

The V-MXene (V_2CT_x and $V_4C_3T_x$) can be synthesized using various top-down approaches. Naguib et al [155] reported two dimensional V_2CT_x synthesized using selective etching of V_2AlC MAX phase in 50% of HF for 90 h. The time required for etching was reduced to 8h by milling MAX powder before intercalating with HF solution. Another report presented the synthesis of V_2C MXene via selective etching using a mixture of LiF + HCl mixture which took 120 h for uniform multilayer and high purity synthesis [156]. Liu et al. [157] prepared V_2C MXene using sodium fluoride and hydrochloric acid as etching agents wherein the time required for transferring uniform MXene was 72 h at 90^0C. Both methods achieved >90% pure V_2C along with decent exfoliation and individual flakes. Wang et al. [158] synthesized 2D multilayered V_4C_3 by selective etching of the Al layer from V_4AlC_3. The MXene they obtained possessed excellent characteristics such as large specific surface area (~31.35 m g^{-1}), high interlayer spacing (~0.466 nm), good pore volumes (~0.047 cm^3g^{-1}), good hydrophilicity and multi valence states of vanadium (+2, +3, and +4). The chemical selective etching of MAX phase using HF acid or LiF + HCl is the most used for the synthesis of V-MXene but higher time consumption for etching and toxic nature of HF is the major challenge where replacement is needed through innovation in the synthesis method.

Apart from V-based MXene, V containing MXene are also synthesized for various applications. To reduce etching time, Wang et al. [159] prepared $(V_x, Ti_{1-x})_2C$ (x = 1, 0.7, 0.5, 0.3, 0) via LiF + HCl mixture for etching process. The addition of Ti reduced the etching time from 120 h to as little as 5 h. In another experiment, $(V_{0.5}Cr_{0.5})_3C_2T_x$ was synthesized from $(V_{0.5}Cr_{0.5})_3AlC_2$ MAX phase using HF etching and it took 69 h for the etching process [160].

4.3 Nb-MXene

Nb-based MXene (TiNbC) was synthesized for the first time in the year 2012 [160]. Using the first principle method, Khazaei et al. [161] studied Nb-MXene and showed that the stability of Nb-MXene is more than the Ti-MXene. The unique catalytic property and biocompatibility characteristics of Nb-MXene attracted the attention of major attention in energy conversion and the medical field [162,163]. Nb_2CTx can be synthesized using three different methods namely, HF acid etching, LiF+HCl mixture etching and hydrothermal methods. Naguib et al.

[164] reported niobium carbide as a promising material for Li-ion battery and synthesised Nb-MXene using HF etching (50% concentration at RT for 90 hrs). Xiao et al. [165] reported Nb_2CTx synthesized using LiF and HCl mixture etching. The analysis of these reports suggests that HF etching is the most effective way of synthesis due to the strong Nb-Al bond. A similar HF method was also used for the synthesis of Nb_4C_3 MXene [166]. Peng et al. [167] reported a hydrothermal route to synthesise Nb-MXene where low-toxicity etching agents (NaBF4, HCl) were used. The MXene obtained from the hydrothermal method showed high-efficiency exfoliation.

Other than pure Nb-MXene, Nb containing MXene have also been synthesized using HF etching such as $TiNbCT_x$ [160], $(Nb_{0.8},Ti_{0.2})_4C_3T_x$ [168], $(Nb_{0.8},Zr_{0.2})_4C_3T_x$ [168], $Nb_{3.5}W_{0.5}C_3T_x$ [169] and $Nb_{3.5}Ta_{0.5}C_3T_x$ [169]. The Nb-containing MXene contains randomly distributed vacancies instead of ordered vacancies and further optimization can be done to synthesise both defective and defect-free Nb-based MXenes.

4.4 Hf-MXene

There are many theoretical reports available in the literature on the study of Hf-MXene materials [170–177]. Zhou et al. [178] synthesized Hf-MXene ($Hf_3C_2T_x$) experimentally by selective etching of a layered parent $Hf_3[Al(Si)]_4C_6$ compound using HF acid. Their characterization results demonstrated a delaminated structure with favourable flexibility. The $Hf_3C_2T_x$ MXene was predicted to be semi-metal with high mechanical strength. Yang et al. [170] reported Hf-MXene for energy storage application using density functional calculations. In this study, various parameters such as possible structures, adsorption energies, electronic structures, charge transfer, average intercalation potential, and diffusion energy barriers were measured.

4.5 Cr-MXene

In 2012, Cr containing MXene was reported for the first time where $(V_{0.5}Cr_{0.5})_3C_2$ was synthesized using 50% HF selective etching method for 69 h. In this synthesis, interlayer spacing (2.426 Å) was seen to be much higher than the Ti_2C [8]. Anasori et al. [179] . synthesized Cr_2TiC_2 MXene using HCl + LiF for 42 h at 55^0C. The results showed that the c-lattice parameter was 24.3Å. Zhau et al. [180] reported a simple strategy for the synthesis of Cr_2CTx by applying H_2SO_4 and LiF composition under gentle conditions. The STEM results demonstrated that the Al layer from the Cr_2AlC MAX phase was etched successfully and transformed to the Cr_2CT_x MXene without fluorine group. Trans et al. [181] attempted to exfoliate Cr_2GaC using HF solution where chromium carbide and oxide were formed but no sign of Cr-MXene formation was seen. Apart from this many research groups have studied Cr-MXene using DFT [182,183].

4.6 Ta-MXene

Ta_4C_3 MXene was synthesized for the first time using the Ta_4AlC_3 MAX phase by 50% concentration HF solution for 72 h [8]. Dai et al. [184] reported tantalum carbide MXene composite for multiple imagining guided

photothermal tumour ablations where Ta_4C_3 MXene was synthesized using 40% HF selective etching for 96 hrs and a further 12 hrs of sonication. In another report, Lin et al. [185] synthesized Ta_4C_3 MXene by HF selective and probe sonication for photothermal ablation of tumours. Tantalum carbide was also used for breast cancer theragnostic by synthesising it using 40% HF selective etching for three days [186]. Ta containing MXene was reported for Li-ion battery by Grace et al. [187] where $Ti_xTa_{(4-x)}AlC_3$ MAX phase was transferred to $Ti_xTa_{(4-x)}C_3$ using 40% HF solution for 4 days.

5. Energy Storage Applications

Recently, electrified transportation and other next-generation smart electrified grid demand for high energy density, power density and excellent life cycle to ensure consistent energy supply and long life [14] are becoming increasingly important. In that context, the development of large-scale energy storage devices is critical to integrating renewable energy sources into high power energy supply [14]. Till now, many energy storage systems have been discovered and developed such as batteries, supercapacitors and fuel cells. Among them, lithium-ion battery, sodium-ion battery, lithium-sulfur battery and supercapacitor are the most famous systems currently being used in the market. However, these energy storage systems are not fully developed and suffers from technological issues such as:

(a) Although lithium-ion batteries possess high energy density, it lacks power density due to slow intercalation. Also, deintercalation of lithium-ion in the electrode material further lowers the rate of intercalation/deintercalation in the solid electrolyte which limits performance.

(b) The intrinsic insulation nature of sulfur in lithium-sulfur batteries hinders its power density performance. Further solubility of discharge product in organic solvent especially, sulfur species can diffuse through separator membrane which can result in the loss of active mass which leads to poor cyclability also called shuttle effect.

(c) Supercapacitors possess good power density and cycle life as compared to the battery and are safer to handle, environmentally friendly and can operate at a wide range of temperatures. The poor energy density of the supercapacitor limits its application in practical life.

To achieve high performance and to mitigate the above-mentioned challenges in energy storage systems, various nano-engineering techniques such as surface modification, controlled morphology and composite formation for 2D MXene are critically needed [14]. Some of these new advances are discussed next.

5.1 Lithium-ion Battery

In the arena of electrified transpiration, Lithium-ion batteries (LIB) are considered potential contenders due to their superior characteristics. Also, power sources for laptops, mobile phones, cameras and other electronic equipment needs rechargeable lithium-ion batteries due to their improved energy density which is 2-3 times higher

energy per weight or volume compared to the conventional batteries [14]. Since 1990, when the first commercialized lithium battery came into existence, continuous research and development have happened in this field. As an anode, graphite material is used more conventionally in LIB because of its excellent properties like higher conductivity, good stability, and cost-effectiveness. However, Li-ion interactions using graphite as an anode result in a maximum specific capacity of 372 $mAhg^{-1}$ [188]. Also, high-rate charge-discharge cycling can degrade the electrochemical properties of LIB. In that context, the development of novel materials or technologies for the enhancement of the electrochemical performance of LIB has become a critical issue. The wide chemical and structural variety of 2D MXene material attracted attention for high-power LIB as compared to the other 2D materials. Gogotsi was among the first to report the possibilities of using MXene for LIB applications [189]. The newly discovered 2D MXene materials demonstrated higher surface area (SSA) which was 10-fold higher than graphene and MAX phase (Ti_2AlC). The higher SSA, open structure and weak interlayer bond between the Ti_2C MXene layer increase the specific capacity of 225 mAh g^{-1}. Also, a Li^+ ion occupies the interlayer between the Ti_2C MXene. Thus, the idea of exploring new MXene family material for LIB electrodes [190] came into being. Further, Naguib et al. [191] reported niobium and vanadium carbides as electrode materials for LIB by removing the Al layer of Nb_2AlC and V_2AlC MAX phases using the chemical selective etching method. The Nb_2C and V_2C showed the reversible capacity of 170 and 260 $mAhg^{-1}$ respectively. Also, both these electrode materials withstood high cycling rates at 10C which showed that the fast Li-ion intercalation and deintercalation for these electrodes is possible.

Theoretical studies have shown that the 2D MXene is a potential candidate for different energy storage electrode materials [192–195]. It has been found that the MXene having low molecular weight such as M_2C (Ti, Nb, V and Sc) are the most potential candidate due to its higher gravimetric capacities [196]. It is assumed that metal ions diffuse between MXene sheets because of the strong bond between M and X [14]. Due to the presence of inactive TiC in Ti_3C_2, poor gravimetric performance was seen in comparison to Ti_2C. Experimental proof on Ti_2CT_x demonstrated that Li^+ uptake higher specific capacity than the $Ti_3C_2T_x$ obtained from the same synthesis method [197]. The research work also showed that the capacity of MXene material is not only decided by its weight [14]. The heavier Nb, Nb_2CT_x showed more specific capacity than Ti_2CT_x which was partially explained by complicated features of ion storage [14]. Furthermore, the properties of the functional groups on the surface of MXene also revealed the performance of MXene materials in the energy storage devices [198,199].

For bare Ti_3C_2 MXene, easy migration of Li-ion was observed due to the low energy barrier and small path length while Ti-MXene with functional terminals on the surface (Ti_3C_2Tx, T_x = -OH, -F) showed a higher diffusion barrier due to the retardation of surface functional groups [54]. The synthesis of MXene using HF selective etching mostly

generated -OH functional group on the surface of MXene and such -OH terminated MXene exhibited poor electrochemical performance for the Li-ion battery. On the other hand, the –O terminal functional group demonstrated the highest Li-ion storage capacity obtained at high-temperature processing from –OH terminated MXenes. These eliminated the dependency of capacity over terminal functional groups of MXene. Furthermore, the Li diffusion barrier calculations also demonstrated high lithium ion mobility in –O terminated MXene owing to favoured lithium-ion transport [190]. Mashtalir et al. [200] reported amine assisted delamination of Nb_2AlC MAX to produce Nb_2CT_x for lithium-ion storage devices and results in prominently –O terminated MXene with highly separated Nb_2CT_x flakes from multilayer stacks. This MXene showed excellent capacity and stability as an electrode for the Li-ion batteries.

Apart from surface functional groups, the surface cations of MXene can greatly affect the LIB performance. With inspiration from the unique metal ion uptake behaviour of Ti_3C_2 MXene [201], Lau et al. [201,202] enhanced capacity by introducing Sn^{4+} ions decorated on Ti_3C_2 via a facile polyvinylpyrrolidone assisted liquid phase immersion process shown in **Figure 8**. Due to the possible pillar effect of Sn between the layers of alk-Ti_3C_2 and the synergistic effect of Sn and MXene, the nanocomposite obtained from the process demonstrated reversible volumetric capacity of 1375 $mAhg^{-1}$ at 216.5$mAcm^{-3}$ current density along with excellent cyclic stability and retention at higher current density. The intercalation theoretical process was discussed for a long time and the key features of the interaction were also experimentally proved afterwards.

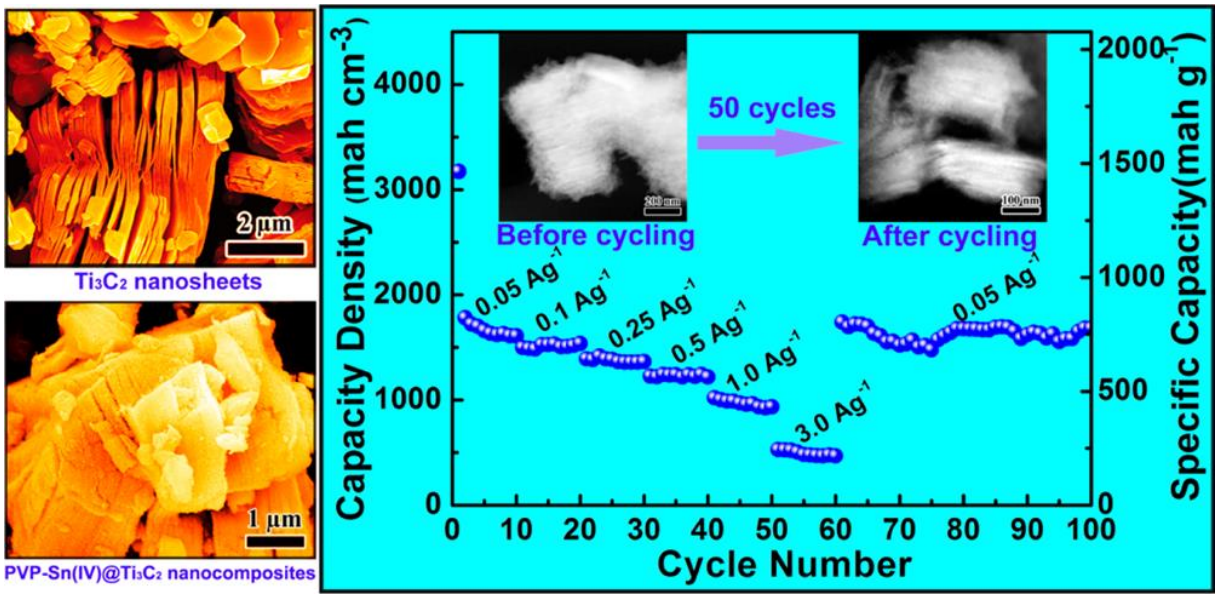

Figure 8 a. SEM images of Sn^{4+} decorated Ti_3C_2 and cyclic performance of nanocomposite [191] Reproduced with permission, © 2015, Wiley Online Library.

To understand the charge storage mechanism of Li-ion in the $Ti_3C_2T_x$, the *in-situ* study was conducted using the X-ray absorption spectroscopy technique [203]. The experimental results demonstrated transition metal oxidation states changed continuously during charge-discharge up to a potential of 0.5V for the Li/Li^+. Further, reduction in voltage did not show any effect on the oxidation state, instead of the additional layer reversibly formed by Li-ion improve the electronic conductivity of MXenes which boost specific capacity and the same mechanism can be applied for other MXene family members.

Further capacity improvement in LIB is possible by optimizing electrode architecture and hybridizing MXene with other electrochemical materials [204,205]. Lin et al. [205] fabricated MXene by growing carbon nanofibers within the gaps of Ti_3C_2Tx particles as well as outsides which avoids interlayer stacking of MXene and prepared Ti_3C_2/CNF demonstrated higher reversible capacity compared with bare Ti_3C_2 MXene

Due to the excellent electronic conductivity of MXene, it enabled reversible ion and electron transport at the interface and prevented the agglomeration of active mass during intercalation and deintercalation. Liu et al. [206] also prepared self-assembled transition metal oxide nanostructure (TiO_2 nanorods and SnO_2 nanowires) on Ti_3C_2 MXene sheets through van der Waals interaction. The TMO nanostructure act as a spacer that avoids restacking of MXene layers which prevents loss of active areas. The fabricated TMO/MXene exhibit extraordinary electrochemical properties for lithium-ion batteries by offering a short diffusion pathway and extra active sites. Other reports on TMO/MXene also have shown excellent performance such as high power/energy and high rate performance material for LIB [207,208].

The metal nanoparticle decorated on MXene also exhibited good performance as anode materials LIB. Zou et al. [209] reported MXene/Ag composite which showed reversible capacities of 310, 260, 150 $mAhg^{-1}$ at 1C, 10C and 50C respectively along with excellent cyclic stability where composite withstand 5000 cycles of 1-50C without capacity decay.

In summary, the lithium storage property in MXene was influenced by various parameters, it has been seen that the surface functional groups, surface decoration forming a composite with other materials can alter the Li-ion battery performance [210]. Hence, rigorous nano-engineering of MXene can lead to innovations in the field of LIB. Hitherto, only limited MXene with few metals have been experimentally tested for LIB, further tuning of component and ratio of metal/carbon of MXene can open a window of opportunity to prepare novel types of LIB.

5.2 MXene Materials for Lithium-Sulfur Battery

To meet the current need for a high-power source for electric vehicles and other applications, continuous progress in the energy storage field is happening. Nowadays, lithium-sulfur battery attracted the attention of researchers due to their rich electrochemical performance as compared to LIB [211–214]. The average potential window for

lithium-sulfur battery lies has rather smaller values (2.2V vs Li^+/Li) as compared to other cathode materials, but sulfur electrode's high specific capacity value can reach up to 1672 $mAhg^{-1}$ while the energy density of 2567 $WhKg^{-1}$ is much higher than other battery technologies [14,215,216].

Though, Li-S demonstrated superior performance in terms of excellent capacity and energy density, the practical utility of Li-S is still challenging due to the drawbacks such as low electrochemical utilization of sulfur and fast capacity fading [14]. The sulfur and sulfur products (Li_2S) generated during discharge of Li-S are ionically and electronically insulating hence trapping of sulfur in conductive materials matrix such as carbon is necessary but it reduces the energy density [14,57]. Another issue with Li-S is the formation of soluble polysulfide intermediate as sulfur undergoes a series of complicated compositional and structural changes and this polysulfide dissolves in organic solvent leading to loss of active mass [14,211–213]. The trapping of sulfur in a conductive carbon matrix can enhance the conductivity of the carbon/sulfur cathode and also the dissolution of polysulfide in an organic solvent can be minimized [14]. The anchoring effect of lithium polysulfide on various 2D layered materials has been studied using computational methods [14]. Anchoring materials can induce strong binding interaction with Li_2S_n species which can minimize dissolution of polysulfide and can enhance cyclability and stability [217]. The computational study showed that MXene possesses the excellent characteristic of the adsorption of Li_2S_x species while binding strength can be determined from the charge transfer number from a cluster of sulfur atoms [218]. The polysulfides such as Li_2S_4, Li_2S_6, and Li_2S_8 can be trapped by bare and hydroxyl-terminated MXene, while LiS_2 and LiS can be confined by –O terminated or bare MXene increases the utilization of active materials of sulfur [14,217]. The outcome of this investigation suggests that the use of S/MXene composites is favourable for Li-S batteries.

Sim et al. [219] studied different mechanisms for trapping the shuttling effect of Ti_2CF_2 and Ti_2CO_2 in Li-S batteries. The shuttling effect in Li-S is restricted by Ti_2CF_2 via strong interaction with LiPSs and Ti_2CO_2 converts highly soluble high order LiPSs into insoluble elemental sulfur. Zhao et al. [220] synthesized layered Ti_3C_2 MXene using 40% HF etching and a composite of S/Ti_3C_2 (**Figure 9 a-f**) was used as a cathode for the Li-S battery. The fabricated Li-S demonstrated an initial discharge capacity of 1291 $mAhg^{-1}$ and the capacity retention of 970 $mAhg^{-1}$ after 100 cycles shown in **Figure 9 g**. Liang et al. [218] reported 2D conductive MXene as host for S/Ti_2C composite for LiS battery, where strong interaction between polysulfide species and Ti on the surface of MXene demonstrated excellent cyclic performance with a specific capacity of approx 1200 $mAhg^{-1}$ at C/5 rate while capacity retention of 80% achieved over 400 cycles. MXene material not only provides a conductive matrix that accommodates volume change upon cycling but also absorbs polysulfide molecules and reduces dissolution of polysulfide in an organic solvent which avoids loss of active mass [14,222].

By using this principle carbon nanotubes interweaved between layers of MXene were not only found to create a porous and high conductivity network but also adsorbs polysulfide generated during discharge product of Li-S. The fabricated MXene/CNT hierarchical structure provides rich loading as a sulfur host with superior electrochemical performance in Li-S battery [223]. Zhang et al. [224] reported lamellar MXene composite with sandwiched CNT which enabled rich loading of sulfur to form multiple physical barriers coupled with chemical trapping suppress the polysulfide dissolution.

More research is going on in order to increase the adsorption of polysulfide on MXene for Li-S batteries by doping nitrogen in MXene [225]. Bao et al. [226] reported crumpled nitrogen-doped MXene nanosheet which introduces heteroatom's in the MXene and this increases SSA, well-defined porosity and large pore volume which results in high areal sulfur loading (5.1 mg cm^{-2}) and strong physical and chemical dual adsorption of polysulfide. Li-S battery based on nitrogen-doped MXene/Sulfur was obtained reversible specific capacity of 1144 $mAhg^{-1}$ at 0.2C rate along with increased stability. Such doping strategy can be applied to other carbide/nitride MXene family members to improve the performance of the Li-S battery [227,228]. To enhance sulfur loading, various approaches are used such as forming a composite with carbon nanotubes or graphene to form a structure with a large pore volume [14].

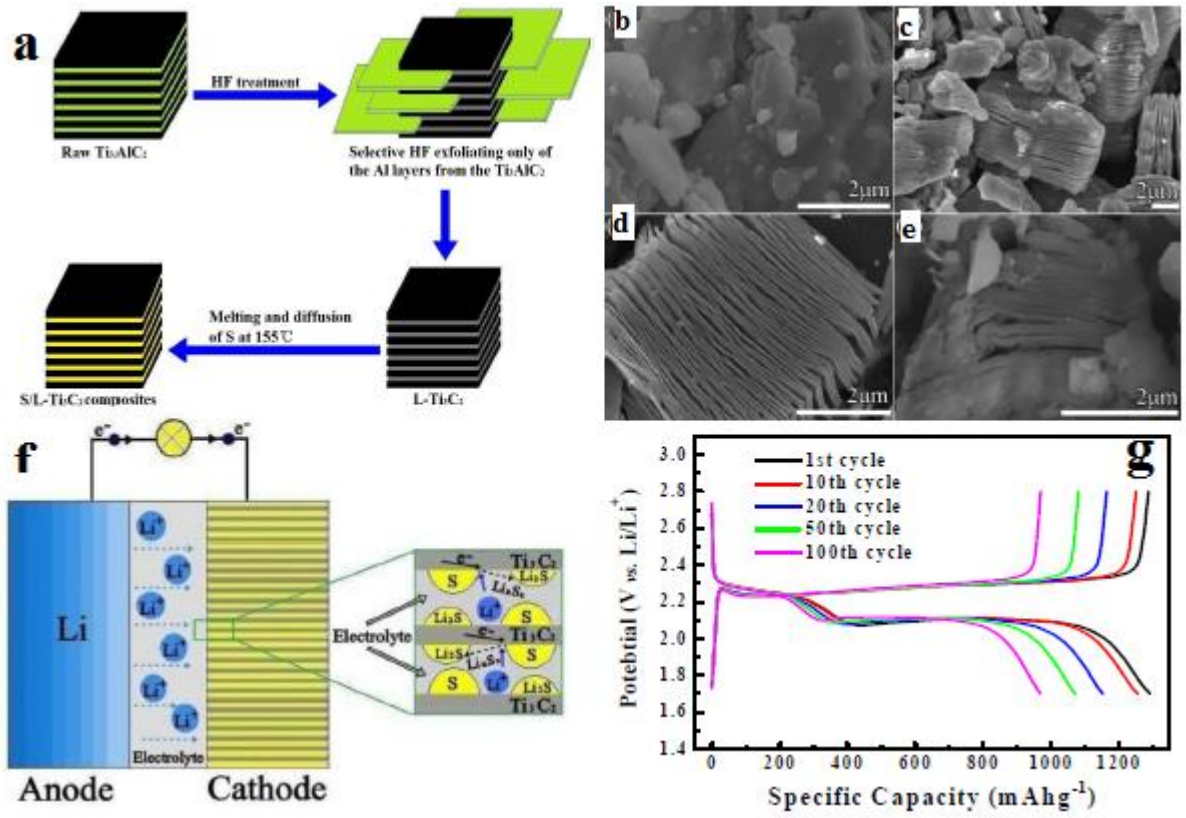

Figure 9 a. Schematic illustration for the synthesis of S/L-Ti_3C_2 b-e. Representative FESEM micrographs of f. Schematic illustration Li-S discharge process g. Galvanostatic charge/discharge curves. [207] Reproduced with permission, © 2015, Royal Society of Chemistry.

Mesoporous carbon having a robust structure provides sufficient space sulfur loading also effective solutions for volumetric expansion during cycling of Li-S battery [229]. To extend the cyclic performance of Li-S, MXenes can be used as additives in the cathode and as membranes [230,231]. Dong et al. [232] fabricated Li-S battery using all MXene based flexible and integrated S cathode where 3D alkalized Ti_3C_2 nanoribbon (MNR) framework as S/polysulfide host while 2D delaminated Ti_3C_2 nanosheet as interlayer on polypropylene separator. The alkalized Ti_3C_2 MNR provides open interconnected macropores and rich surface area which not only increases S loading but also enhances ionic diffusion while 2D delaminated Ti_3C_2 reduces the shuttle effect of lithium polysulfide. The electrode as cathode did not use Al foil as a substrate which demonstrated excellent reversible capacity, rate capacity and low overpotential for Li-S battery.

Further, Zhang et al. [233] synthesized sulfur cathode for Li-S where single-atom zinc implanted in MXene was introduced, which catalyze the conversion reaction of polysulfide by reducing the energy barrier from Li_2S_4 to Li_2S_2/Li_2S. Also, due to the high electronegativity of atomic Zn on MXene, it creates strong interaction with polysulfide. In another report, AlF_3 and $Ni(OH)_2$ was introduced on $Ti_3C_2T_x$ MXene, where AlF_3 nanoparticles dispersed on the surface and at inter-layers of MXene exhibited strong chemisorption's of polysulfide while decorated $Ni(OH)_2$ nanosheet plays as a baffle and effectively limits the migration of soluble polysulfide and improves its redox kinetics [234]. Also, Qui et al. [235] reported MXene@TiO_2 heterostructures to dual chemisorption of lithium polysulfide to achieve a high-performance Li-S battery.

In summary, as compared with the conventional conductive host for sulfur such as carbon-based materials, MXene is more instinctive in polarization which effectively entraps polysulfide during cycling of Li-S battery. MXene with surface terminals can further improve the adsorption quantity of polysulfide which reduces the shuttling effect of the Li-S battery. Further, to increase sulfur loading, different approaches like forming a composite with carbon-based materials or interweaving carbon material in between layers have been used.

5.3 MXene Material for Supercapacitor

Supercapacitors have attracted widespread attention due to their high power density, extended life cycle and high rate performance [236]. Typically, based on charge storage mechanism supercapacitors are classified into two categories: electric double-layer capacitors (EDLC) and pseudocapacitors [237]. EDLC stores charge electrostatically at the electrode/electrolyte interface via physical ion adsorption/desorption process forming

Helmholtz layer [236,238,239]. Ideally, EDLC represents rectangular cyclic voltammograms without signs of redox thumb demonstrate excellent power performance. While charges are stored at the surface only the energy density for EDLC is limited (~10 Wh kg^{-1}) due to the limited electrode surface area [240,241]. On the other hand, pseudocapacitor is the potential alternative for EDLC due to its high charge storing capacity through reversible redox reaction [242]. The transition metal oxide used for the pseudocapacitor suffers from poor electronic conductivity while conductive polymers have poor stability and such drawbacks of pseudocapacitor limit its practical applications [243].

Two-dimensional MXene family materials have great potential as high-performance supercapacitor electrodes due to their extraordinary electronic conductivity, layered structure, chemical and physical stability and mechanical flexibility [244,245]. The variety of oxidation states of transition metals enables intrinsic conductive and feasibility of charge transfer, also the unique layered structure of MXene deliver excellent electrochemical properties, thereby beneficial for energy storage [240]. Other advantages of MXene are the possibility to intercalate with both polar organic and metallic ions [14]. The chemical and electrochemical intercalation of a wide variety of mono-/multi-valent cations like Li^+, Na^+, K^+, Mg^+ and NH^{4+} into MXene are possible which can deliver high volume capacity [14,244,246]. The excellent electronic conductivity of MXene provides fast electronic charge transfer to other active masses which can improve the electronic performance of the composites [14]. An in-situ study conducted using XAS demonstrated that the MXene coupled with oxide has shown pseudocapacitive behaviour [247]. In ions adsorption, the functional groups at the surface of MXene (-O, -OH, -F) also plays an important role which improved volume capacity [248].

Appropriate design of MXene material is critical for high-performance supercapacitor electrode materials [14]. Particularly, the interlayer spacing of MXene, porosity and the functional groups on the surface plays a vital role in deciding the electrochemical performance of the supercapacitor. Ma et al [249] reported lignosulfonates (LS) modified $Ti_3C_2T_x$ MXene for supercapacitor where P-Π conjugated structure of LS endows α and β carbon a strong chemical reactivity and local positive potential which improve the surface of MXene also avoid the restacking issue. Xu et al. [250] reported that ionic insertion and exchange and ionic diffusion in MXene leads to charge storage through fast counter-ion insertion and counter ion/co-ion exchange during charge-discharge. Also, increasing interlayer spacing facilitates the organic molecules and metal ions in the supercapacitor. The hydrazine intercalation into MXene (2D titanium carbide) leads to changes in MXene surface chemistry by reducing the amount of -OH groups and intercalated water [251]. Also, the pillaring effect was observed where preopening the structure and improving accessibility of actives sides occurred. Since the discovery of MXene, Ti_3C_2Tx has been extensively researched for supercapacitor electrode applications. Ghidiu et al. [252] reported 2D titanium carbide

clay for super capacitive applications exhibited volumetric capacitance much higher than the other carbon-based materials still reported.

The $Ti_3C_2T_x$ MXene prepared in this report used lithium fluoride and hydrochloric acid, and the material was observed to swell due to the hydration and the film obtained (see **Figure 10 a-b** [253]). The 1.1 um thick film delivered ultra-high volumetric capacitance along with rate capacity (**Figure 10 c-g**).

The cyclability test performed on $Ti_3C_2T_x$ showed that all MXene based microsupercapacitor exhibited 100% capacitance retention even after 10,000 cycles at a scan rate of 50 mVs^{-1} [254]. The areal and volumetric capacitance of 27 $mFcm^{-2}$ and 357 $mFcm^{-3}$ was obtained for this on-chip device based on MXene material. Tang et al. [250] reported an optimized ion pathway for $Ti_3C_2T_x$ MXene for high-performance supercapacitor where the H_2SO_4 oxidation method was used to avoid restacking in MXene.

In order to understand volumetric changes in MXene upon cycling Jackel et al. [255] conducted in-situ X-ray studies to observe volumetric changes in MXene in contact with different ionic liquids. Results obtained from this study showed that during first contact of ionic liquid drastic, initial and irreversible volume expansion occurred and further swelling and shrinkage occur upon cycling. Hence to maintain a stratified structure, a stable interlayer is helpful. To improve capacitance one of the ways is the lamination of conjugated polymers.

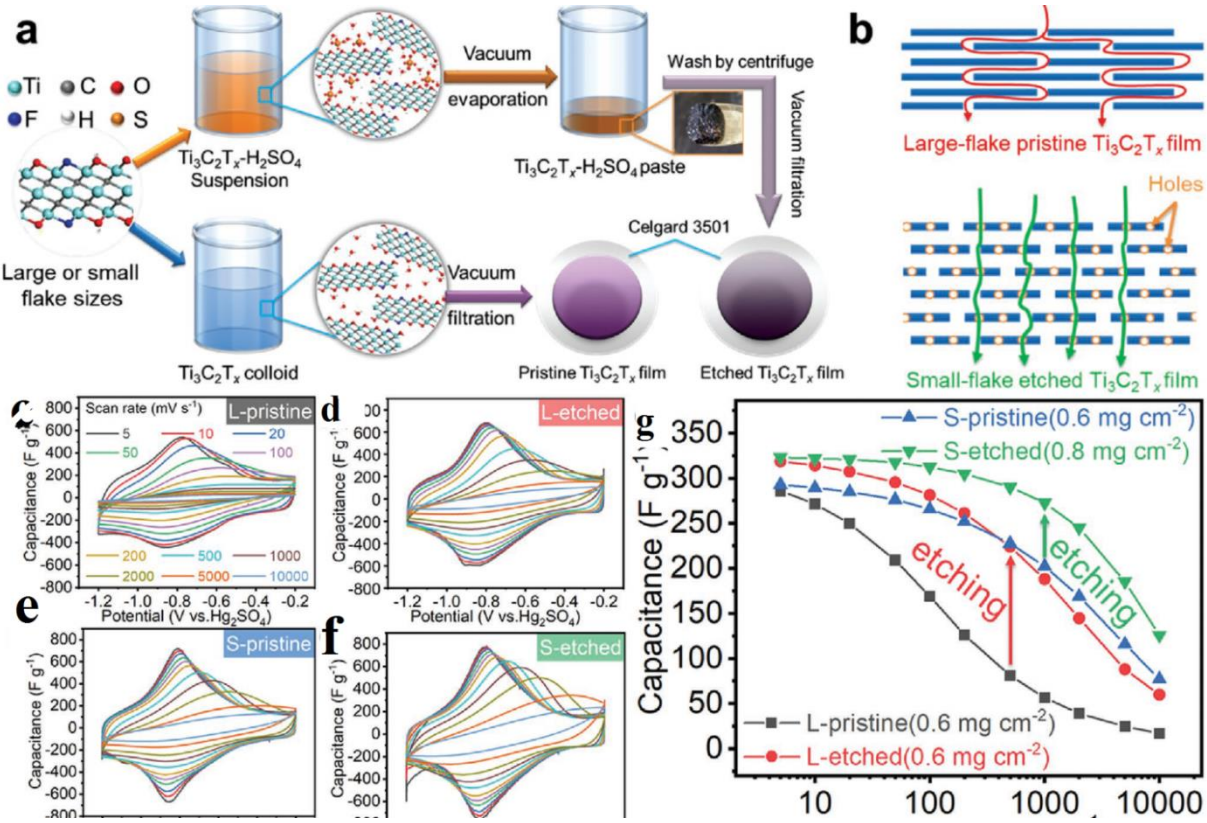

Figure 10 a. Schematic illustrations of the etching process of $Ti_3C_2T_x$ nanosheets and the obtained hierarchical nanoporous structure b. The schematic illustration of the ion pathway optimization in S-etched Ti_3C_2Tx film comparing with the L-pristine film. c-g. Comparison of electrochemical performance of $Ti_3C_2T_x$ films before and after etching.[253] Reproduced with permission, © 2021, Wiley Online Library.

Boota et al. [256] demonstrated that polar polymer (polyfluorene) with charge, nitrogen-containing ends have the strongest interaction with $Ti_3C_2T_x$ layers and yielded increased interlayer spacing leads to enhancement in volumetric capacitance. In order to enhance ion transport, many strategies are applied such as increasing interlayer spacing, introducing film porosity by designing nanoarchitecture, but these strategies limit volumetric energy storage as well as become complex and lengthy ion transport path hinders the charge-discharge rate [257]. To achieve thickness independent electrochemical performance, the vertical alignments of two-dimensional flakes are necessary which can enable directional ion transport [257]. Using this approach resulting MXene electrode film demonstrated excellent film independent performance up to film thickness of 200 um.

The surface modification approach offers new horizons in improving electrochemical performance [258]. The conductivity of MXene is affected by the presence of surface functional groups [57]. Recently using methods such as alkalization and calcination, it is possible to synthesise MXene without a surface functional group. The bare MXene exhibited superior electronic conductivity with the improved electrochemical performance of the supercapacitor [259].

Gaun et al. [260] synthesized uniform multilayered and high purity V_2C MXene using HF-free method and these exhibited specific capacitance of 164 Fg^{-1}, good cyclic stability along 90% capacitance retention after 10,000 cycles. Lukatskaya et al. [261] demonstrated that the two-dimensional transition metal carbides can operate at a higher rate than conventional EDLC. Even though at a high rate, such MXene exhibit higher volumetric and areal capacitance than the EDLC, transition metal oxide and conducting polymer materials electrodes. Two different architectures were fabricated such as macroporous Ti_3C_2Tx MXene film exhibited 210 Fg^{-1} which is higher than best carbon supercapacitor performance while MXene hydrogel exhibited volumetric capacitance of 1500 Fcm^{-3} higher than the previously reported performance of RuO_2. Wang et al. [262] reported a chemical interface tailored regulation strategy to unravel and alleviate self-discharge behaviour of $Ti_3C_2T_x$ MXene based supercapacitor. The results showed that a decrease in F elements can decline the positive self-discharge rate.

The computational study showed that doping of cation or anion can modify MXene by reducing band gap which leads to enhancement in electrochemical performance of supercapacitor. Balci et al. [263] demonstrated modification of bandgap in the Sc_2CF_2 through carbon replacement with Sn, F, N, B, Si, Ge and (N+B). By

introducing dopant, the Sn bandgap of Sc_2CF_2 was reduced from 0.96 to 0.24 eV. In other cases, by doping of nitrogen in $Ti_3C_2T_x$, changed the c lattice parameter from 1.92 to 2.46 nm. Due to this doping process, surface area increases and electrochemical activity sites result in an enhanced electrochemical process [264,265].

The MXene materials are not only used for liquid electrolyte-based supercapacitors but also used in solid-state supercapacitors [266]. The characteristic high elastic moduli when the force applied in one direction of MXene becomes the potential candidate for an all-solid-state supercapacitor [267]. Zhang et al [268] synthesized highly transparent and conductive $Ti_3C_2T_x$ films by using spin casting and annealing method for transparent solid-state supercapacitor. The film thickness of 4 nm with transparency of 93% and DC conductivity 5736 Scm^{-1} demonstrated excellent volumetric capacitance with a faster response. Also, asymmetric supercapacitor developed from $Ti_3C_2T_x$ (transparency 72%) film with SWCNT showed high capacitance and extended life cycle with no capacitance retention till 20,000 cycles. Zhuo et al. [269] synthesized $Ti_3C_2T_x$/rGO composite for supercapacitor which combined the electrochemical and mechanical properties of $Ti_3C_2T_x$ and mechanical robustness of rGO. The symmetric supercapacitor assembled from this composite delivered a specific capacitance of 18.6 mF cm^{-2} and stretchability of up to 300%.

In summary, to enhance the electrochemical performance of supercapacitor, various approaches such as interlayer adjustment, surface modification, modification using dopant and combining with other special materials can be used [14]. Using these approaches, tremendous changes in MXene layers are found which improves the capacitance and energy density of the supercapacitor. Further, the use of MXene in solid-state supercapacitors has shown excellent areal as well as volumetric capacitance [14]. However, there is still further scope to develop a supercapacitor with high energy density while maintaining power density.

6. Conclusions and Future Perspectives

This review highlights the progress made in the development and synthesis methods to fabricate the newly emerging family of two-dimensional MXene materials. The first part of the review covers synthesis methods other than the conventional HF selective etching method. Further, development in MXene family members other than Ti-MXene material is also discussed. The other part of the review covers the applications of MXene for energy storage applications which includes applications for Li-ion battery, Li-S battery and supercapacitor and different approaches in improving electrochemical performance are discussed. Though extensive research has been done on MXene materials in the past decades, still many challenges limit its use in practical applications which are discussed in this section.

With the help of computational techniques more than hundreds of MXene compositions are predicted by considering terminal groups and multi-elements, and yet so many MXene members are waiting to be developed

experimentally. MXene members developed computationally need to synthesise precursors for that ternary carbide such as Hf_2C, Sc_2C or W_2C etc. Hence, the development of a new MAX phase and layered nitride or carbide precursor become the major challenge to developing new MXene members.

The second challenge is the green synthesis method for the preparation of MXene. Recently, many HF-free MXene synthesis methods have been discovered but the major challenge is the synthesis of thin 2D materials through an effective exfoliation method. The thickness reduction affects the reactivity of 2D materials as it increases specific surface area. The functional group plays a vital role in electrochemical performance, as the presence of the functional groups convert metal MXenes into semiconductors. Hence control of functional groups on the surface of MXene during synthesis is another major challenge. To achieve higher electrochemical performance, tuning morphology is also a vital method that increases active sites. Further, porosity control and curvature not only enhance active sites through increasing surface area and pore volume but also enhance the performance of the energy storage device. Synthesis of defect-free or without functional group electrode materials for Li-ion battery can achieve high initial Coulombic efficiency. In the case of Li-S battery, shuttle effect is the major challenge which can be controlled by using Mxene as cathode where MXene trap maximum polysulfide molecule. For supercapacitors, high specific surface area and good conductivity are major constraints that can be achieved by introducing high porosity and avoiding function groups during the synthesis of MXenes.

Acknowledgements

PL received a postdoctoral fellowship from Savitribai Phule Pune University under the SPPU postdoc fellowship scheme. SG greatly acknowledge the financial support provided by the UKRI via Grants No. EP/S036180/1 and EP/T024607/1, Transforming the Foundation Industries NetworkPlus Feasibility study award to LSBU (EP/V026402/1), the Royal Academy of Engineering via Grants No. IAPP18-19\295 and TSP1332, The Hubert Curien Partnership award 2022 from the British Council and the Newton Fellowship award from the Royal Society (NIF\R1\191571). Wherever applicable the work made use of Isambard Bristol, UK supercomputing service accessed by a Resource Allocation Panel (RAP) grant as well as ARCHER2 resources (Project e648).

References

[1] M. Naguib, M.W. Barsoum, Y. Gogotsi, Ten Years of Progress in the Synthesis and Development of MXenes, Adv. Mater. 33 (2021) 2103393. https://doi.org/10.1002/adma.202103393.

[2] S. Misra, N.K. Katiyar, A. Kumar, S. Goel, K. Biswas, Nanofabrication route to achieve sustainable production of next generation defect-free graphene: analysis and characterisation, Nanofabrication. 6 (2021) 36–43. https://doi.org/10.1515/nanofab-2020-0101.

[3] P. Saravanan, S. Rajeswari, J.A. Kumar, M. Rajasimman, N. Rajamohan, Bibliometric analysis and recent trends on MXene research – A comprehensive review, Chemosphere. 286 (2022) 131873. https://doi.org/10.1016/j.chemosphere.2021.131873.

[4] J.A. Kumar, P. Prakash, T. Krithiga, D.J. Amarnath, J. Premkumar, N. Rajamohan, Y. Vasseghian, P. Saravanan, M. Rajasimman, Methods of synthesis, characteristics, and environmental applications of MXene: A comprehensive review, Chemosphere. 286 (2022) 131607. https://doi.org/10.1016/j.chemosphere.2021.131607.

[5] P. Dhiman, G. Rana, A. Kumar, G. Sharma, D.-V.N. Vo, Mu. Naushad, ZnO-based heterostructures as photocatalysts for hydrogen generation and depollution: a review, Environ. Chem. Lett. (2022). https://doi.org/10.1007/s10311-021-01361-1.

[6] R. Garg, A. Agarwal, M. Agarwal, A review on MXene for energy storage application: effect of interlayer distance, Mater. Res. Express. 7 (2020) 022001. https://doi.org/10.1088/2053-1591/ab750d.

[7] M. Naguib, M. Kurtoglu, V. Presser, J. Lu, J. Niu, M. Heon, L. Hultman, Y. Gogotsi, M.W. Barsoum, Two-Dimensional Nanocrystals Produced by Exfoliation of Ti3AlC2, Adv. Mater. 23 (2011) 4248–4253. https://doi.org/10.1002/adma.201102306.

[8] M. Naguib, O. Mashtalir, J. Carle, V. Presser, J. Lu, L. Hultman, Y. Gogotsi, M.W. Barsoum, Two-Dimensional Transition Metal Carbides, ACS Nano. 6 (2012) 1322–1331. https://doi.org/10.1021/nn204153h.

[9] M. Naguib, O. Mashtalir, J. Carle, V. Presser, J. Lu, L. Hultman, Y. Gogotsi, M.W. Barsoum, Two-Dimensional Transition Metal Carbides, ACS Nano. 6 (2012) 1322–1331. https://doi.org/10.1021/nn204153h.

[10] N.C. Frey, J. Wang, G.I. Vega Bellido, B. Anasori, Y. Gogotsi, V.B. Shenoy, Prediction of Synthesis of 2D Metal Carbides and Nitrides (MXenes) and Their Precursors with Positive and Unlabeled Machine Learning, ACS Nano. 13 (2019) 3031–3041. https://doi.org/10.1021/acsnano.8b08014.

[11] Y. Sheth, S. Dharaskar, V. Chaudhary, M. Khalid, R. Walvekar, Prospects of titanium carbide-based MXene in heavy metal ion and radionuclide adsorption for wastewater remediation: A review, Chemosphere. 293 (2022) 133563. https://doi.org/10.1016/j.chemosphere.2022.133563.

[12] V. Thirumal, R. Yuvakkumar, P.S. Kumar, G. Ravi, S.P. Keerthana, D. Velauthapillai, Facile single-step synthesis of MXene@CNTs hybrid nanocomposite by CVD method to remove hazardous pollutants, Chemosphere. 286 (2022) 131733. https://doi.org/10.1016/j.chemosphere.2021.131733.

[13] M. Naguib, J. Come, B. Dyatkin, V. Presser, P.-L. Taberna, P. Simon, M.W. Barsoum, Y. Gogotsi, MXene: a promising transition metal carbide anode for lithium-ion batteries, Electrochem. Commun. 16 (2012) 61–64. https://doi.org/10.1016/j.elecom.2012.01.002.

[14] J. Nan, X. Guo, J. Xiao, X. Li, W. Chen, W. Wu, H. Liu, Y. Wang, M. Wu, G. Wang, Nanoengineering of 2D MXene-Based Materials for Energy Storage Applications, Small. 17 (2021) 1902085. https://doi.org/10.1002/smll.201902085.

[15] X. Tang, X. Guo, W. Wu, G. Wang, 2D Metal Carbides and Nitrides (MXenes) as High-Performance Electrode Materials for Lithium-Based Batteries, Adv. Energy Mater. 8 (2018) 1801897. https://doi.org/10.1002/aenm.201801897.

[16] C. Chen, X. Xie, B. Anasori, A. Sarycheva, T. Makaryan, M. Zhao, P. Urbankowski, L. Miao, J. Jiang, Y. Gogotsi, MoS_2-on-MXene Heterostructures as Highly Reversible Anode Materials for Lithium-Ion Batteries, Angew. Chem. Int. Ed. 57 (2018) 1846–1850. https://doi.org/10.1002/anie.201710616.

[17] D. Zhao, Z. Chen, W. Yang, S. Liu, X. Zhang, Y. Yu, W.-C. Cheong, L. Zheng, F. Ren, G. Ying, X. Cao, D. Wang, Q. Peng, G. Wang, C. Chen, MXene (Ti_3C_2) Vacancy-Confined Single-Atom Catalyst for Efficient Functionalization of CO_2, J. Am. Chem. Soc. 141 (2019) 4086–4093. https://doi.org/10.1021/jacs.8b13579.

[18] J. Zhang, Y. Zhao, X. Guo, C. Chen, C.-L. Dong, R.-S. Liu, C.-P. Han, Y. Li, Y. Gogotsi, G. Wang, Single platinum atoms immobilized on an MXene as an efficient catalyst for the hydrogen evolution reaction, Nat. Catal. 1 (2018) 985–992. https://doi.org/10.1038/s41929-018-0195-1.

[19] J. Guo, J. Huo, Y. Liu, W. Wu, Y. Wang, M. Wu, H. Liu, G. Wang, Nitrogen-Doped Porous Carbon Supported Nonprecious Metal Single-Atom Electrocatalysts: from Synthesis to Application, Small Methods. 3 (2019) 1900159. https://doi.org/10.1002/smtd.201900159.

[20] C.-F. Du, K.N. Dinh, Q. Liang, Y. Zheng, Y. Luo, J. Zhang, Q. Yan, Self-Assemble and In Situ Formation of $Ni_{1-x}Fe_xPS_3$ Nanomosaic-Decorated MXene Hybrids for Overall Water Splitting, Adv. Energy Mater. 8 (2018) 1801127. https://doi.org/10.1002/aenm.201801127.

[21] C. Du, X. Sun, H. Yu, Q. Liang, K.N. Dinh, Y. Zheng, Y. Luo, Z. Wang, Q. Yan, Synergy of Nb Doping and Surface Alloy Enhanced on Water–Alkali Electrocatalytic Hydrogen Generation Performance in Ti-Based MXene, Adv. Sci. (2019) 1900116. https://doi.org/10.1002/advs.201900116.

[22] Y. Xie, Y. Dall'Agnese, M. Naguib, Y. Gogotsi, M.W. Barsoum, H.L. Zhuang, P.R.C. Kent, Prediction and Characterization of MXene Nanosheet Anodes for Non-Lithium-Ion Batteries, ACS Nano. 8 (2014) 9606–9615. https://doi.org/10.1021/nn503921j.

[23] M. Naguib, J. Halim, J. Lu, K.M. Cook, L. Hultman, Y. Gogotsi, M.W. Barsoum, New Two-Dimensional Niobium and Vanadium Carbides as Promising Materials for Li-Ion Batteries, J. Am. Chem. Soc. 135 (2013) 15966–15969. https://doi.org/10.1021/ja405735d.

[24] R.B. Rakhi, B. Ahmed, M.N. Hedhili, D.H. Anjum, H.N. Alshareef, Effect of Postetch Annealing Gas Composition on the Structural and Electrochemical Properties of Ti_2CT_x MXene Electrodes for Supercapacitor Applications, Chem. Mater. 27 (2015) 5314–5323. https://doi.org/10.1021/acs.chemmater.5b01623.

[25] M.R. Lukatskaya, O. Mashtalir, C.E. Ren, Y. Dall'Agnese, P. Rozier, P.L. Taberna, M. Naguib, P. Simon, M.W. Barsoum, Y. Gogotsi, Cation Intercalation and High Volumetric Capacitance of Two-Dimensional Titanium Carbide, Science. 341 (2013) 1502–1505. https://doi.org/10.1126/science.1241488.

[26] Z.W. Seh, K.D. Fredrickson, B. Anasori, J. Kibsgaard, A.L. Strickler, M.R. Lukatskaya, Y. Gogotsi, T.F. Jaramillo, A. Vojvodic, Two-Dimensional Molybdenum Carbide (MXene) as an Efficient Electrocatalyst for Hydrogen Evolution, ACS Energy Lett. 1 (2016) 589–594. https://doi.org/10.1021/acsenergylett.6b00247.

[27] J. Halim, M.R. Lukatskaya, K.M. Cook, J. Lu, C.R. Smith, L.-Å. Näslund, S.J. May, L. Hultman, Y. Gogotsi, P. Eklund, M.W. Barsoum, Transparent Conductive Two-Dimensional Titanium Carbide Epitaxial Thin Films, Chem. Mater. 26 (2014) 2374–2381. https://doi.org/10.1021/cm500641a.

[28] M. Mariano, O. Mashtalir, F.Q. Antonio, W.-H. Ryu, B. Deng, F. Xia, Y. Gogotsi, A.D. Taylor, Solution-processed titanium carbide MXene films examined as highly transparent conductors, Nanoscale. 8 (2016) 16371–16378. https://doi.org/10.1039/C6NR03682A.

[29] Y. Yang, S. Umrao, S. Lai, S. Lee, Large-Area Highly Conductive Transparent Two-Dimensional Ti_2CT_x Film, J. Phys. Chem. Lett. 8 (2017) 859–865. https://doi.org/10.1021/acs.jpclett.6b03064.

[30] S. Lai, J. Jeon, S.K. Jang, J. Xu, Y.J. Choi, J.-H. Park, E. Hwang, S. Lee, Surface group modification and carrier transport properties of layered transition metal carbides (Ti_2CT_x, T: –OH, –F and –O), Nanoscale. 7 (2015) 19390–19396. https://doi.org/10.1039/C5NR06513E.

[31] F. Shahzad, M. Alhabeb, C.B. Hatter, B. Anasori, S. Man Hong, C.M. Koo, Y. Gogotsi, Electromagnetic interference shielding with 2D transition metal carbides (MXenes), Science. 353 (2016) 1137–1140. https://doi.org/10.1126/science.aag2421.

[32] J. Liu, H.-B. Zhang, R. Sun, Y. Liu, Z. Liu, A. Zhou, Z.-Z. Yu, Hydrophobic, Flexible, and Lightweight MXene Foams for High-Performance Electromagnetic-Interference Shielding, Adv. Mater. 29 (2017) 1702367. https://doi.org/10.1002/adma.201702367.

[33] O. Mashtalir, K.M. Cook, V.N. Mochalin, M. Crowe, M.W. Barsoum, Y. Gogotsi, Dye adsorption and decomposition on two-dimensional titanium carbide in aqueous media, J Mater Chem A. 2 (2014) 14334–14338. https://doi.org/10.1039/C4TA02638A.

[34] Z.W. Seh, K.D. Fredrickson, B. Anasori, J. Kibsgaard, A.L. Strickler, M.R. Lukatskaya, Y. Gogotsi, T.F. Jaramillo, A. Vojvodic, Two-Dimensional Molybdenum Carbide (MXene) as an Efficient Electrocatalyst for Hydrogen Evolution, ACS Energy Lett. 1 (2016) 589–594. https://doi.org/10.1021/acsenergylett.6b00247.

[35] A. Kumar, S.K. Sharma, G. Sharma, C. Guo, D.-V.N. Vo, J. Iqbal, Mu. Naushad, F.J. Stadler, Silicate glass matrix@Cu2O/Cu2V2O7 p-n heterojunction for enhanced visible light photo-degradation of sulfamethoxazole: High charge separation and interfacial transfer, J. Hazard. Mater. 402 (2021) 123790. https://doi.org/10.1016/j.jhazmat.2020.123790.

[36] S.K. Sharma, A. Kumar, G. Sharma, D.-V.N. Vo, A. García-Peñas, O. Moradi, M. Sillanpää, MXenes based nano-heterojunctions and composites for advanced photocatalytic environmental detoxification and energy conversion: A review, Chemosphere. 291 (2022) 132923. https://doi.org/10.1016/j.chemosphere.2021.132923.

[37] G. Fan, X. Li, Y. Ma, Y. Zhang, J. Wu, B. Xu, T. Sun, D. Gao, J. Bi, Magnetic, recyclable $Pt_yCo_{1-y}/Ti_3C_2X_2$ (X = O, F) catalyst: a facile synthesis and enhanced catalytic activity for hydrogen generation from the hydrolysis of ammonia borane, New J. Chem. 41 (2017) 2793–2799. https://doi.org/10.1039/C6NJ02695H.

[38] J. Guo, Q. Peng, H. Fu, G. Zou, Q. Zhang, Heavy-Metal Adsorption Behavior of Two-Dimensional Alkalization-Intercalated MXene by First-Principles Calculations, J. Phys. Chem. C. 119 (2015) 20923–20930. https://doi.org/10.1021/acs.jpcc.5b05426.

[39] Q. Peng, J. Guo, Q. Zhang, J. Xiang, B. Liu, A. Zhou, R. Liu, Y. Tian, Unique Lead Adsorption Behavior of Activated Hydroxyl Group in Two-Dimensional Titanium Carbide, J. Am. Chem. Soc. 136 (2014) 4113–4116. https://doi.org/10.1021/ja500506k.

[40] X. Yu, Y. Li, J. Cheng, Z. Liu, Q. Li, W. Li, X. Yang, B. Xiao, Monolayer Ti_2CO_2: A Promising Candidate for NH_3 Sensor or Capturer with High Sensitivity and Selectivity, ACS Appl. Mater. Interfaces. 7 (2015) 13707–13713. https://doi.org/10.1021/acsami.5b03737.

[41] X. Zhang, J. Xu, H. Wang, J. Zhang, H. Yan, B. Pan, J. Zhou, Y. Xie, Ultrathin Nanosheets of MAX Phases with Enhanced Thermal and Mechanical Properties in Polymeric Compositions: $Ti_3Si_{0.75}Al_{0.25}C_2$, Angew. Chem. Int. Ed. 52 (2013) 4361–4365. https://doi.org/10.1002/anie.201300285.

[42] M. Xue, Z. Wang, F. Yuan, X. Zhang, W. Wei, H. Tang, C. Li, Preparation of $TiO_2/Ti_3C_2T_x$ hybrid nanocomposites and their tribological properties as base oil lubricant additives, RSC Adv. 7 (2017) 4312–4319. https://doi.org/10.1039/C6RA27653A.

[43] J. Chen, K. Chen, D. Tong, Y. Huang, J. Zhang, J. Xue, Q. Huang, T. Chen, CO_2 and temperature dual responsive "Smart" MXene phases, Chem. Commun. 51 (2015) 314–317. https://doi.org/10.1039/C4CC07220K.

[44] O. Mashtalir, K.M. Cook, V.N. Mochalin, M. Crowe, M.W. Barsoum, Y. Gogotsi, Dye adsorption and decomposition on two-dimensional titanium carbide in aqueous media, J Mater Chem A. 2 (2014) 14334–14338. https://doi.org/10.1039/C4TA02638A.

[45] F. Liu, A. Zhou, J. Chen, H. Zhang, J. Cao, L. Wang, Q. Hu, Preparation and methane adsorption of two-dimensional carbide Ti2C, Adsorption. 22 (2016) 915–922. https://doi.org/10.1007/s10450-016-9795-8.

[46] M. Fu, P. Tamarat, H. Huang, J. Even, A.L. Rogach, B. Lounis, Neutral and Charged Exciton Fine Structure in Single Lead Halide Perovskite Nanocrystals Revealed by Magneto-optical Spectroscopy, Nano Lett. 17 (2017) 2895–2901. https://doi.org/10.1021/acs.nanolett.7b00064.

[47] Q. Hu, D. Sun, Q. Wu, H. Wang, L. Wang, B. Liu, A. Zhou, J. He, MXene: A New Family of Promising Hydrogen Storage Medium, J. Phys. Chem. A. 117 (2013) 14253–14260. https://doi.org/10.1021/jp409585v.

[48] Q. Hu, H. Wang, Q. Wu, X. Ye, A. Zhou, D. Sun, L. Wang, B. Liu, J. He, Two-dimensional Sc2C: A reversible and high-capacity hydrogen storage material predicted by first-principles calculations, Int. J. Hydrog. Energy. 39 (2014) 10606–10612. https://doi.org/10.1016/j.ijhydene.2014.05.037.

[49] J.-J. Zhang, S. Dong, Superconductivity of monolayer Mo_2C: The key role of functional groups, J. Chem. Phys. 146 (2017) 034705. https://doi.org/10.1063/1.4974085.

[50] L.-Y. Gan, D. Huang, U. Schwingenschlögl, Oxygen adsorption and dissociation during the oxidation of monolayer Ti2C, J. Mater. Chem. A. 1 (2013) 13672. https://doi.org/10.1039/c3ta12032e.

[51] C. Ling, L. Shi, Y. Ouyang, Q. Chen, J. Wang, Transition Metal-Promoted V_2CO_2 (MXenes): A New and Highly Active Catalyst for Hydrogen Evolution Reaction, Adv. Sci. 3 (2016) 1600180. https://doi.org/10.1002/advs.201600180.

[52] C. Ling, L. Shi, Y. Ouyang, J. Wang, Searching for Highly Active Catalysts for Hydrogen Evolution Reaction Based on O-Terminated MXenes through a Simple Descriptor, Chem. Mater. 28 (2016) 9026–9032. https://doi.org/10.1021/acs.chemmater.6b03972.

[53] B. Anasori, J.G. Gogocij, eds., 2D metal carbides and nitrides (MXenes): structure, properties and applications, Springer, Cham, 2019.

[54] R. Garg, A. Agarwal, M. Agarwal, A review on MXene for energy storage application: effect of interlayer distance, Mater. Res. Express. 7 (2020) 022001. https://doi.org/10.1088/2053-1591/ab750d.

[55] M. Khazaei, A. Ranjbar, M. Arai, T. Sasaki, S. Yunoki, Electronic properties and applications of MXenes: a theoretical review, J. Mater. Chem. C. 5 (2017) 2488–2503. https://doi.org/10.1039/C7TC00140A.

[56] M. Naguib, M.W. Barsoum, Y. Gogotsi, Ten Years of Progress in the Synthesis and Development of MXenes, Adv. Mater. 33 (2021) 2103393. https://doi.org/10.1002/adma.202103393.

[57] B. Anasori, M.R. Lukatskaya, Y. Gogotsi, 2D metal carbides and nitrides (MXenes) for energy storage, Nat. Rev. Mater. 2 (2017) 16098. https://doi.org/10.1038/natrevmats.2016.98.

[58] A.N. Enyashin, A.L. Ivanovskii, Atomic structure, comparative stability and electronic properties of hydroxylated Ti2C and Ti3C2 nanotubes, Comput. Theor. Chem. 989 (2012) 27–32. https://doi.org/10.1016/j.comptc.2012.02.034.

[59] M. Naguib, M. Kurtoglu, V. Presser, J. Lu, J. Niu, M. Heon, L. Hultman, Y. Gogotsi, M.W. Barsoum, Two-Dimensional Nanocrystals Produced by Exfoliation of Ti3AlC2, Adv. Mater. 23 (2011) 4248–4253. https://doi.org/10.1002/adma.201102306.

[60] O. Mashtalir, M. Naguib, V.N. Mochalin, Y. Dall'Agnese, M. Heon, M.W. Barsoum, Y. Gogotsi, Intercalation and delamination of layered carbides and carbonitrides, Nat. Commun. 4 (2013) 1716. https://doi.org/10.1038/ncomms2664.

[61] Q. Tang, Z. Zhou, P. Shen, Are MXenes Promising Anode Materials for Li Ion Batteries? Computational Studies on Electronic Properties and Li Storage Capability of Ti_3C_2 and $Ti_3C_2X_2$ (X = F, OH) Monolayer, J. Am. Chem. Soc. 134 (2012) 16909–16916. https://doi.org/10.1021/ja308463r.

[62] Z.M. Sun, Progress in research and development on MAX phases: a family of layered ternary compounds, Int. Mater. Rev. 56 (2011) 143–166. https://doi.org/10.1179/1743280410Y.0000000001.

[63] M. Barsoum, T. El-Raghy, The MAX Phases: Unique New Carbide and Nitride Materials, Am. Sci. 89 (2001) 334. https://doi.org/10.1511/2001.28.736.

[64] M. Yoshida, Y. Hoshiyama, J. Ommyoji, A. Yamaguchi, Reaction mechanism for the synthesis of Ti3AlC2 through an intermediate carbide of Ti3AlC from elemental Ti, Al, and C powder mixture, J. Ceram. Soc. Jpn. 118 (2010) 37–42. https://doi.org/10.2109/jcersj2.118.37.

[65] X. Li, Z. Huang, C. Zhi, Environmental Stability of MXenes as Energy Storage Materials, Front. Mater. 6 (2019) 312. https://doi.org/10.3389/fmats.2019.00312.

[66] M. Malaki, A. Maleki, R.S. Varma, MXenes and ultrasonication, J. Mater. Chem. A. 7 (2019) 10843–10857. https://doi.org/10.1039/C9TA01850F.

[67] P. Simon, Two-Dimensional MXene with Controlled Interlayer Spacing for Electrochemical Energy Storage, ACS Nano. 11 (2017) 2393–2396. https://doi.org/10.1021/acsnano.7b01108.

[68] T.Y. Ma, J.L. Cao, M. Jaroniec, S.Z. Qiao, Interacting Carbon Nitride and Titanium Carbide Nanosheets for High-Performance Oxygen Evolution, Angew. Chem. Int. Ed. 55 (2016) 1138–1142. https://doi.org/10.1002/anie.201509758.

[69] N.K. Chaudhari, H. Jin, B. Kim, D. San Baek, S.H. Joo, K. Lee, MXene: an emerging two-dimensional material for future energy conversion and storage applications, J. Mater. Chem. A. 5 (2017) 24564–24579. https://doi.org/10.1039/C7TA09094C.

[70] O. Mashtalir, M.R. Lukatskaya, A.I. Kolesnikov, E. Raymundo-Piñero, M. Naguib, M.W. Barsoum, Y. Gogotsi, The effect of hydrazine intercalation on the structure and capacitance of 2D titanium carbide (MXene), Nanoscale. 8 (2016) 9128–9133. https://doi.org/10.1039/C6NR01462C.

[71] M. Ghidiu, M.R. Lukatskaya, M.-Q. Zhao, Y. Gogotsi, M.W. Barsoum, Conductive two-dimensional titanium carbide 'clay' with high volumetric capacitance, Nature. 516 (2014) 78–81. https://doi.org/10.1038/nature13970.

[72] O. Mashtalir, M. Naguib, V.N. Mochalin, Y. Dall'Agnese, M. Heon, M.W. Barsoum, Y. Gogotsi, Intercalation and delamination of layered carbides and carbonitrides, Nat. Commun. 4 (2013) 1716. https://doi.org/10.1038/ncomms2664.

[73] M. Malaki, A. Maleki, R.S. Varma, MXenes and ultrasonication, J. Mater. Chem. A. 7 (2019) 10843–10857. https://doi.org/10.1039/C9TA01850F.

[74] M. Naguib, V.N. Mochalin, M.W. Barsoum, Y. Gogotsi, 25th Anniversary Article: MXenes: A New Family of Two-Dimensional Materials, Adv. Mater. 26 (2014) 992–1005. https://doi.org/10.1002/adma.201304138.

[75] L. Verger, V. Natu, M. Carey, M.W. Barsoum, MXenes: An Introduction of Their Synthesis, Select Properties, and Applications, Trends Chem. 1 (2019) 656–669. https://doi.org/10.1016/j.trechm.2019.04.006.

[76] L. Zhao, B. Li, Synthesis and recent applications of MXenes with Mo, V or Nb transition metals: a review, Tungsten. 2 (2020) 176–193. https://doi.org/10.1007/s42864-020-00048-4.

[77] C. Xu, L. Wang, Z. Liu, L. Chen, J. Guo, N. Kang, X.-L. Ma, H.-M. Cheng, W. Ren, Large-area high-quality 2D ultrathin Mo2C superconducting crystals, Nat. Mater. 14 (2015) 1135–1141. https://doi.org/10.1038/nmat4374.

[78] C. Xu, L. Wang, Z. Liu, L. Chen, J. Guo, N. Kang, X.-L. Ma, H.-M. Cheng, W. Ren, Large-area high-quality 2D ultrathin Mo2C superconducting crystals, Nat. Mater. 14 (2015) 1135–1141. https://doi.org/10.1038/nmat4374.

[79] D. Geng, X. Zhao, Z. Chen, W. Sun, W. Fu, J. Chen, W. Liu, W. Zhou, K.P. Loh, Direct Synthesis of Large-Area 2D Mo_2C on In Situ Grown Graphene, Adv. Mater. 29 (2017) 1700072. https://doi.org/10.1002/adma.201700072.

[80] Y. Gogotsi, Transition metal carbides go 2D, Nat. Mater. 14 (2015) 1079–1080. https://doi.org/10.1038/nmat4386.

[81] L. Ma, L.R.L. Ting, V. Molinari, C. Giordano, B.S. Yeo, Efficient hydrogen evolution reaction catalyzed by molybdenum carbide and molybdenum nitride nanocatalysts synthesized via the urea glass route, J. Mater. Chem. A. 3 (2015) 8361–8368. https://doi.org/10.1039/C5TA00139K.

[82] I.R. Shein, A.L. Ivanovskii, Graphene-like titanium carbides and nitrides Tin+1Cn, Tin+1Nn (n=1, 2, and 3) from de-intercalated MAX phases: First-principles probing of their structural, electronic properties and relative stability, Comput. Mater. Sci. 65 (2012) 104–114. https://doi.org/10.1016/j.commatsci.2012.07.011.

[83] P. Urbankowski, B. Anasori, T. Makaryan, D. Er, S. Kota, P.L. Walsh, M. Zhao, V.B. Shenoy, M.W. Barsoum, Y. Gogotsi, Synthesis of two-dimensional titanium nitride Ti_4N_3 (MXene), Nanoscale. 8 (2016) 11385–11391. https://doi.org/10.1039/C6NR02253G.

[84] J. Mei, G.A. Ayoko, C. Hu, J.M. Bell, Z. Sun, Two-dimensional fluorine-free mesoporous Mo2C MXene via UV-induced selective etching of Mo2Ga2C for energy storage, Sustain. Mater. Technol. 25 (2020) e00156. https://doi.org/10.1016/j.susmat.2020.e00156.

[85] M.A. Ali, M.R. Khatun, N. Jahan, M.M. Hossain, Comparative study of Mo_2Ga_2C with superconducting *MAX* phase Mo_2GaC: First-principles calculations, Chin. Phys. B. 26 (2017) 033102. https://doi.org/10.1088/1674-1056/26/3/033102.

[86] T. Li, L. Yao, Q. Liu, J. Gu, R. Luo, J. Li, X. Yan, W. Wang, P. Liu, B. Chen, W. Zhang, W. Abbas, R. Naz, D. Zhang, Fluorine-Free Synthesis of High-Purity $Ti_3C_2T_x$ (T=OH, O) via Alkali Treatment, Angew. Chem. Int. Ed. 57 (2018) 6115–6119. https://doi.org/10.1002/anie.201800887.

[87] S. Yang, P. Zhang, F. Wang, A.G. Ricciardulli, M.R. Lohe, P.W.M. Blom, X. Feng, Fluoride-Free Synthesis of Two-Dimensional Titanium Carbide (MXene) Using A Binary Aqueous System, Angew. Chem. 130 (2018) 15717–15721. https://doi.org/10.1002/ange.201809662.

[88] M. Alhabeb, K. Maleski, B. Anasori, P. Lelyukh, L. Clark, S. Sin, Y. Gogotsi, Guidelines for Synthesis and Processing of Two-Dimensional Titanium Carbide ($Ti_3C_2T_x$ MXene), Chem. Mater. 29 (2017) 7633–7644. https://doi.org/10.1021/acs.chemmater.7b02847.

[89] M. Naguib, O. Mashtalir, M.R. Lukatskaya, B. Dyatkin, C. Zhang, V. Presser, Y. Gogotsi, M.W. Barsoum, One-step synthesis of nanocrystalline transition metal oxides on thin sheets of disordered graphitic carbon by oxidation of MXenes, Chem Commun. 50 (2014) 7420–7423. https://doi.org/10.1039/C4CC01646G.

[90] H. Ghassemi, W. Harlow, O. Mashtalir, M. Beidaghi, M.R. Lukatskaya, Y. Gogotsi, M.L. Taheri, In situ environmental transmission electron microscopy study of oxidation of two-dimensional Ti_3C_2 and formation of carbon-supported TiO_2, J. Mater. Chem. A. 2 (2014) 14339. https://doi.org/10.1039/C4TA02583K.

[91] Z. Li, L. Wang, D. Sun, Y. Zhang, B. Liu, Q. Hu, A. Zhou, Synthesis and thermal stability of two-dimensional carbide MXene Ti3C2, Mater. Sci. Eng. B. 191 (2015) 33–40. https://doi.org/10.1016/j.mseb.2014.10.009.

[92] J. Li, Y. Du, C. Huo, S. Wang, C. Cui, Thermal stability of two-dimensional Ti2C nanosheets, Ceram. Int. 41 (2015) 2631–2635. https://doi.org/10.1016/j.ceramint.2014.10.070.

[93] L. Verger, V. Natu, M. Carey, M.W. Barsoum, MXenes: An Introduction of Their Synthesis, Select Properties, and Applications, Trends Chem. 1 (2019) 656–669. https://doi.org/10.1016/j.trechm.2019.04.006.

[94] J. Pang, R.G. Mendes, A. Bachmatiuk, L. Zhao, H.Q. Ta, T. Gemming, H. Liu, Z. Liu, M.H. Rummeli, Applications of 2D MXenes in energy conversion and storage systems, Chem. Soc. Rev. 48 (2019) 72–133. https://doi.org/10.1039/C8CS00324F.

[95] M. Khazaei, M. Arai, T. Sasaki, C.-Y. Chung, N.S. Venkataramanan, M. Estili, Y. Sakka, Y. Kawazoe, Novel Electronic and Magnetic Properties of Two-Dimensional Transition Metal Carbides and Nitrides, Adv. Funct. Mater. 23 (2013) 2185–2192. https://doi.org/10.1002/adfm.201202502.

[96] M. Khazaei, A. Ranjbar, M. Arai, T. Sasaki, S. Yunoki, Electronic properties and applications of MXenes: a theoretical review, J. Mater. Chem. C. 5 (2017) 2488–2503. https://doi.org/10.1039/C7TC00140A.

[97] M. Ashton, K. Mathew, R.G. Hennig, S.B. Sinnott, Predicted Surface Composition and Thermodynamic Stability of MXenes in Solution, J. Phys. Chem. C. 120 (2016) 3550–3556. https://doi.org/10.1021/acs.jpcc.5b11887.

[98] M. Khazaei, A. Ranjbar, M. Arai, S. Yunoki, Topological insulators in the ordered double transition metals M 2 ′ M ″ C 2 MXenes (M ′ = Mo , W; M ″ = Ti , Zr, Hf), Phys. Rev. B. 94 (2016) 125152. https://doi.org/10.1103/PhysRevB.94.125152.

[99] M. Khazaei, M. Arai, T. Sasaki, A. Ranjbar, Y. Liang, S. Yunoki, OH-terminated two-dimensional transition metal carbides and nitrides as ultralow work function materials, Phys. Rev. B. 92 (2015) 075411. https://doi.org/10.1103/PhysRevB.92.075411.

[100] T. Hu, J. Wang, H. Zhang, Z. Li, M. Hu, X. Wang, Vibrational properties of Ti_3C_2 and $Ti_3C_2T_2$ (T = O, F, OH) monosheets by first-principles calculations: a comparative study, Phys. Chem. Chem. Phys. 17 (2015) 9997–10003. https://doi.org/10.1039/C4CP05666C.

[101] Y. Xie, M. Naguib, V.N. Mochalin, M.W. Barsoum, Y. Gogotsi, X. Yu, K.-W. Nam, X.-Q. Yang, A.I. Kolesnikov, P.R.C. Kent, Role of Surface Structure on Li-Ion Energy Storage Capacity of Two-Dimensional Transition-Metal Carbides, J. Am. Chem. Soc. 136 (2014) 6385–6394. https://doi.org/10.1021/ja501520b.

[102] J.-C. Lei, X. Zhang, Z. Zhou, Recent advances in MXene: Preparation, properties, and applications, Front. Phys. 10 (2015) 276–286. https://doi.org/10.1007/s11467-015-0493-x.

[103] Y. Xie, Y. Dall'Agnese, M. Naguib, Y. Gogotsi, M.W. Barsoum, H.L. Zhuang, P.R.C. Kent, Prediction and Characterization of MXene Nanosheet Anodes for Non-Lithium-Ion Batteries, ACS Nano. 8 (2014) 9606–9615. https://doi.org/10.1021/nn503921j.

[104] C.J. Zhang, S. Pinilla, N. McEvoy, C.P. Cullen, B. Anasori, E. Long, S.-H. Park, A. Seral-Ascaso, A. Shmeliov, D. Krishnan, C. Morant, X. Liu, G.S. Duesberg, Y. Gogotsi, V. Nicolosi, Oxidation Stability of Colloidal Two-Dimensional Titanium Carbides (MXenes), Chem. Mater. 29 (2017) 4848–4856. https://doi.org/10.1021/acs.chemmater.7b00745.

[105] K.A. Papadopoulou, A. Chroneos, D. Parfitt, S.-R.G. Christopoulos, A perspective on MXenes: Their synthesis, properties, and recent applications, J. Appl. Phys. 128 (2020) 170902. https://doi.org/10.1063/5.0021485.
[106] M. Khazaei, M. Arai, T. Sasaki, C.-Y. Chung, N.S. Venkataramanan, M. Estili, Y. Sakka, Y. Kawazoe, Novel Electronic and Magnetic Properties of Two-Dimensional Transition Metal Carbides and Nitrides, Adv. Funct. Mater. 23 (2013) 2185–2192. https://doi.org/10.1002/adfm.201202502.
[107] C. Si, J. You, W. Shi, J. Zhou, Z. Sun, Quantum spin Hall phase in $Mo_2M_2C_3O_2$ (M = Ti, Zr, Hf) MXenes, J. Mater. Chem. C. 4 (2016) 11524–11529. https://doi.org/10.1039/C6TC04560J.
[108] C. Si, K.-H. Jin, J. Zhou, Z. Sun, F. Liu, Large-Gap Quantum Spin Hall State in MXenes: *d* -Band Topological Order in a Triangular Lattice, Nano Lett. 16 (2016) 6584–6591. https://doi.org/10.1021/acs.nanolett.6b03118.
[109] L. Li, Lattice dynamics and electronic structures of Ti3C2O2 and Mo2TiC2O2 (MXenes): The effect of Mo substitution, Comput. Mater. Sci. 124 (2016) 8–14. https://doi.org/10.1016/j.commatsci.2016.07.008.
[110] M. Khazaei, A. Ranjbar, M. Arai, S. Yunoki, Topological insulators in the ordered double transition metals M 2 ′ M ″ C 2 MXenes (M ′ = Mo , W; M ″ = Ti , Zr, Hf), Phys. Rev. B. 94 (2016) 125152. https://doi.org/10.1103/PhysRevB.94.125152.
[111] H. Weng, A. Ranjbar, Y. Liang, Z. Song, M. Khazaei, S. Yunoki, M. Arai, Y. Kawazoe, Z. Fang, X. Dai, Large-gap two-dimensional topological insulator in oxygen functionalized MXene, Phys. Rev. B. 92 (2015) 075436. https://doi.org/10.1103/PhysRevB.92.075436.
[112] H. Zhang, G. Yang, X. Zuo, H. Tang, Q. Yang, G. Li, Computational studies on the structural, electronic and optical properties of graphene-like MXenes (M_2CT_2 , M = Ti, Zr, Hf; T = O, F, OH) and their potential applications as visible-light driven photocatalysts, J. Mater. Chem. A. 4 (2016) 12913–12920. https://doi.org/10.1039/C6TA04628B.
[113] X.-H. Zha, K. Luo, Q. Li, Q. Huang, J. He, X. Wen, S. Du, Role of the surface effect on the structural, electronic and mechanical properties of the carbide MXenes, EPL Europhys. Lett. 111 (2015) 26007. https://doi.org/10.1209/0295-5075/111/26007.
[114] Y. Bai, K. Zhou, N. Srikanth, J.H.L. Pang, X. He, R. Wang, Dependence of elastic and optical properties on surface terminated groups in two-dimensional MXene monolayers: a first-principles study, RSC Adv. 6 (2016) 35731–35739. https://doi.org/10.1039/C6RA03090D.
[115] M. Magnuson, J. Halim, L.-Å. Näslund, Chemical bonding in carbide MXene nanosheets, J. Electron Spectrosc. Relat. Phenom. 224 (2018) 27–32. https://doi.org/10.1016/j.elspec.2017.09.006.
[116] P. Chakraborty, T. Das, D. Nafday, L. Boeri, T. Saha-Dasgupta, Manipulating the mechanical properties of Ti 2 C MXene: Effect of substitutional doping, Phys. Rev. B. 95 (2017) 184106. https://doi.org/10.1103/PhysRevB.95.184106.
[117] U. Yorulmaz, A. Özden, N.K. Perkgöz, F. Ay, C. Sevik, Vibrational and mechanical properties of single layer MXene structures: a first-principles investigation, Nanotechnology. 27 (2016) 335702. https://doi.org/10.1088/0957-4484/27/33/335702.
[118] O. Mashtalir, K.M. Cook, V.N. Mochalin, M. Crowe, M.W. Barsoum, Y. Gogotsi, Dye adsorption and decomposition on two-dimensional titanium carbide in aqueous media, J Mater Chem A. 2 (2014) 14334–14338. https://doi.org/10.1039/C4TA02638A.
[119] B. Anasori, M.R. Lukatskaya, Y. Gogotsi, 2D metal carbides and nitrides (MXenes) for energy storage, Nat. Rev. Mater. 2 (2017) 16098. https://doi.org/10.1038/natrevmats.2016.98.
[120] S. Zhao, W. Kang, J. Xue, Manipulation of electronic and magnetic properties of M_2C (M = Hf, Nb, Sc, Ta, Ti, V, Zr) monolayer by applying mechanical strains, Appl. Phys. Lett. 104 (2014) 133106. https://doi.org/10.1063/1.4870515.
[121] G. Gao, G. Ding, J. Li, K. Yao, M. Wu, M. Qian, Monolayer MXenes: promising half-metals and spin gapless semiconductors, Nanoscale. 8 (2016) 8986–8994. https://doi.org/10.1039/C6NR01333C.
[122] J. Hu, B. Xu, C. Ouyang, S.A. Yang, Y. Yao, Investigations on V_2C and V_2CX_2 (X = F, OH) Monolayer as a Promising Anode Material for Li Ion Batteries from First-Principles Calculations, J. Phys. Chem. C. 118 (2014) 24274–24281. https://doi.org/10.1021/jp507336x.
[123] C. Si, J. Zhou, Z. Sun, Half-Metallic Ferromagnetism and Surface Functionalization-Induced Metal–Insulator Transition in Graphene-like Two-Dimensional Cr_2C Crystals, ACS Appl. Mater. Interfaces. 7 (2015) 17510–17515. https://doi.org/10.1021/acsami.5b05401.
[124] G. Wang, Theoretical Prediction of the Intrinsic Half-Metallicity in Surface-Oxygen-Passivated Cr_2N MXene, J. Phys. Chem. C. 120 (2016) 18850–18857. https://doi.org/10.1021/acs.jpcc.6b05224.
[125] M. Khazaei, M. Arai, T. Sasaki, C.-Y. Chung, N.S. Venkataramanan, M. Estili, Y. Sakka, Y. Kawazoe, Novel Electronic and Magnetic Properties of Two-Dimensional Transition Metal Carbides and Nitrides, Adv. Funct. Mater. 23 (2013) 2185–2192. https://doi.org/10.1002/adfm.201202502.
[126] J. Yang, X. Luo, S. Zhang, L. Chen, Investigation of magnetic and electronic properties of transition metal doped Sc_2CT_2 (T = O, OH or F) using a first principles study, Phys. Chem. Chem. Phys. 18 (2016) 12914–12919. https://doi.org/10.1039/C6CP00138F.

[127] J. Yang, X. Zhou, X. Luo, S. Zhang, L. Chen, Tunable electronic and magnetic properties of $Cr_2M'C_2T_2$ (M′ = Ti or V; T = O, OH or F), Appl. Phys. Lett. 109 (2016) 203109. https://doi.org/10.1063/1.4967983.
[128] G. Ying, S. Kota, A.D. Dillon, A.T. Fafarman, M.W. Barsoum, Conductive transparent V 2 CT x (MXene) films, FlatChem. 8 (2018) 25–30. https://doi.org/10.1016/j.flatc.2018.03.001.
[129] M. Naguib, V.N. Mochalin, M.W. Barsoum, Y. Gogotsi, 25th Anniversary Article: MXenes: A New Family of Two-Dimensional Materials, Adv. Mater. 26 (2014) 992–1005. https://doi.org/10.1002/adma.201304138.
[130] Y. Gogotsi, B. Anasori, The Rise of MXenes, ACS Nano. 13 (2019) 8491–8494. https://doi.org/10.1021/acsnano.9b06394.
[131] Z. Wang, N. Zhang, M. Yu, J. Liu, S. Wang, J. Qiu, Boosting redox activity on MXene-induced multifunctional collaborative interface in high Li2S loading cathode for high-energy Li-S and metallic Li-free rechargeable batteries, J. Energy Chem. 37 (2019) 183–191. https://doi.org/10.1016/j.jechem.2019.03.012.
[132] M. Lu, W. Han, H. Li, W. Zhang, B. Zhang, There is plenty of space in the MXene layers: The confinement and fillings, J. Energy Chem. 48 (2020) 344–363. https://doi.org/10.1016/j.jechem.2020.02.032.
[133] V. Natu, J.L. Hart, M. Sokol, H. Chiang, M.L. Taheri, M.W. Barsoum, Edge Capping of 2D-MXene Sheets with Polyanionic Salts To Mitigate Oxidation in Aqueous Colloidal Suspensions, Angew. Chem. Int. Ed. 58 (2019) 12655–12660. https://doi.org/10.1002/anie.201906138.
[134] C.J. Zhang, S. Pinilla, N. McEvoy, C.P. Cullen, B. Anasori, E. Long, S.-H. Park, A. Seral-Ascaso, A. Shmeliov, D. Krishnan, C. Morant, X. Liu, G.S. Duesberg, Y. Gogotsi, V. Nicolosi, Oxidation Stability of Colloidal Two-Dimensional Titanium Carbides (MXenes), Chem. Mater. 29 (2017) 4848–4856. https://doi.org/10.1021/acs.chemmater.7b00745.
[135] K. Maleski, V.N. Mochalin, Y. Gogotsi, Dispersions of Two-Dimensional Titanium Carbide MXene in Organic Solvents, Chem. Mater. 29 (2017) 1632–1640. https://doi.org/10.1021/acs.chemmater.6b04830.
[136] D. Geng, X. Zhao, Z. Chen, W. Sun, W. Fu, J. Chen, W. Liu, W. Zhou, K.P. Loh, Direct Synthesis of Large-Area 2D Mo_2C on In Situ Grown Graphene, Adv. Mater. 29 (2017) 1700072. https://doi.org/10.1002/adma.201700072.
[137] T.L. Tan, H.M. Jin, M.B. Sullivan, B. Anasori, Y. Gogotsi, High-Throughput Survey of Ordering Configurations in MXene Alloys Across Compositions and Temperatures, ACS Nano. 11 (2017) 4407–4418. https://doi.org/10.1021/acsnano.6b08227.
[138] M. Naguib, J. Halim, J. Lu, K.M. Cook, L. Hultman, Y. Gogotsi, M.W. Barsoum, New Two-Dimensional Niobium and Vanadium Carbides as Promising Materials for Li-Ion Batteries, J. Am. Chem. Soc. 135 (2013) 15966–15969. https://doi.org/10.1021/ja405735d.
[139] J. Lei, A. Kutana, B.I. Yakobson, Predicting stable phase monolayer Mo_2C (MXene), a superconductor with chemically-tunable critical temperature, J. Mater. Chem. C. 5 (2017) 3438–3444. https://doi.org/10.1039/C7TC00789B.
[140] C. Hu, C.-C. Lai, Q. Tao, J. Lu, J. Halim, L. Sun, J. Zhang, J. Yang, B. Anasori, J. Wang, Y. Sakka, L. Hultman, P. Eklund, J. Rosen, M.W. Barsoum, Mo_2Ga_2C: a new ternary nanolaminated carbide, Chem. Commun. 51 (2015) 6560–6563. https://doi.org/10.1039/C5CC00980D.
[141] J. Halim, S. Kota, M.R. Lukatskaya, M. Naguib, M.-Q. Zhao, E.J. Moon, J. Pitock, J. Nanda, S.J. May, Y. Gogotsi, M.W. Barsoum, Synthesis and Characterization of 2D Molybdenum Carbide (MXene), Adv. Funct. Mater. 26 (2016) 3118–3127. https://doi.org/10.1002/adfm.201505328.
[142] S. Joshi, Q. Wang, A. Puntambekar, V. Chakrapani, Facile Synthesis of Large Area Two-Dimensional Layers of Transition-Metal Nitride and Their Use as Insertion Electrodes, ACS Energy Lett. 2 (2017) 1257–1262. https://doi.org/10.1021/acsenergylett.7b00240.
[143] X. Xu, Z. Zhang, L. Qiu, J. Zhuang, L. Zhang, H. Wang, C. Liao, H. Song, R. Qiao, P. Gao, Z. Hu, L. Liao, Z. Liao, D. Yu, E. Wang, F. Ding, H. Peng, K. Liu, Ultrafast growth of single-crystal graphene assisted by a continuous oxygen supply, Nat. Nanotechnol. 11 (2016) 930–935. https://doi.org/10.1038/nnano.2016.132.
[144] X. Lu, M.I.B. Utama, J. Lin, X. Gong, J. Zhang, Y. Zhao, S.T. Pantelides, J. Wang, Z. Dong, Z. Liu, W. Zhou, Q. Xiong, Large-Area Synthesis of Monolayer and Few-Layer $MoSe_2$ Films on SiO_2 Substrates, Nano Lett. 14 (2014) 2419–2425. https://doi.org/10.1021/nl5000906.
[145] I. Bilgin, F. Liu, A. Vargas, A. Winchester, M.K.L. Man, M. Upmanyu, K.M. Dani, G. Gupta, S. Talapatra, A.D. Mohite, S. Kar, Chemical Vapor Deposition Synthesized Atomically Thin Molybdenum Disulfide with Optoelectronic-Grade Crystalline Quality, ACS Nano. 9 (2015) 8822–8832. https://doi.org/10.1021/acsnano.5b02019.
[146] Q. Zhang, J. Lu, Z. Wang, Z. Dai, Y. Zhang, F. Huang, Q. Bao, W. Duan, M.S. Fuhrer, C. Zheng, Reliable Synthesis of Large-Area Monolayer WS_2 Single Crystals, Films, and Heterostructures with

Extraordinary Photoluminescence Induced by Water Intercalation, Adv. Opt. Mater. 6 (2018) 1701347. https://doi.org/10.1002/adom.201701347.

[147] M. Wang, S.K. Jang, W.-J. Jang, M. Kim, S.-Y. Park, S.-W. Kim, S.-J. Kahng, J.-Y. Choi, R.S. Ruoff, Y.J. Song, S. Lee, A Platform for Large-Scale Graphene Electronics - CVD Growth of Single-Layer Graphene on CVD-Grown Hexagonal Boron Nitride, Adv. Mater. 25 (2013) 2746–2752. https://doi.org/10.1002/adma.201204904.

[148] D. Geng, X. Zhao, Z. Chen, W. Sun, W. Fu, J. Chen, W. Liu, W. Zhou, K.P. Loh, Direct Synthesis of Large-Area 2D Mo_2C on In Situ Grown Graphene, Adv. Mater. 29 (2017) 1700072. https://doi.org/10.1002/adma.201700072.

[149] W. Sun, X. Wang, J. Feng, T. Li, Y. Huan, J. Qiao, L. He, D. Ma, Controlled synthesis of 2D Mo_2C/graphene heterostructure on liquid Au substrates as enhanced electrocatalytic electrodes, Nanotechnology. 30 (2019) 385601. https://doi.org/10.1088/1361-6528/ab2c0d.

[150] G. Sun, H. Chang, G. Zhang, B. Yan, K. Chou, A low-cost and efficient pathway for preparation of 2D MoN nanosheets via Na_2CO_3-assisted nitridation of MoS_2 with NH_3, J. Am. Ceram. Soc. 102 (2019) 7178–7186. https://doi.org/10.1111/jace.16649.

[151] C. Xu, L. Wang, Z. Liu, L. Chen, J. Guo, N. Kang, X.-L. Ma, H.-M. Cheng, W. Ren, Large-area high-quality 2D ultrathin Mo2C superconducting crystals, Nat. Mater. 14 (2015) 1135–1141. https://doi.org/10.1038/nmat4374.

[152] S. Chaitoglou, T. Giannakopoulou, T. Speliotis, A. Vavouliotis, C. Trapalis, A. Dimoulas, Mo_2C/graphene heterostructures: low temperature chemical vapor deposition on liquid bimetallic Sn–Cu and hydrogen evolution reaction electrocatalytic properties, Nanotechnology. 30 (2019) 125401. https://doi.org/10.1088/1361-6528/aaf9e8.

[153] H. Lind, J. Halim, S.I. Simak, J. Rosen, Investigation of vacancy-ordered M o 1.33 C MXene from first principles and x-ray photoelectron spectroscopy, Phys. Rev. Mater. 1 (2017) 044002. https://doi.org/10.1103/PhysRevMaterials.1.044002.

[154] Q. Tao, M. Dahlqvist, J. Lu, S. Kota, R. Meshkian, J. Halim, J. Palisaitis, L. Hultman, M.W. Barsoum, P.O.Å. Persson, J. Rosen, Two-dimensional Mo1.33C MXene with divacancy ordering prepared from parent 3D laminate with in-plane chemical ordering, Nat. Commun. 8 (2017) 14949. https://doi.org/10.1038/ncomms14949.

[155] M. Naguib, J. Halim, J. Lu, K.M. Cook, L. Hultman, Y. Gogotsi, M.W. Barsoum, New Two-Dimensional Niobium and Vanadium Carbides as Promising Materials for Li-Ion Batteries, J. Am. Chem. Soc. 135 (2013) 15966–15969. https://doi.org/10.1021/ja405735d.

[156] Y. Guan, S. Jiang, Y. Cong, J. Wang, Z. Dong, Q. Zhang, G. Yuan, Y. Li, X. Li, A hydrofluoric acid-free synthesis of 2D vanadium carbide (V_2C) MXene for supercapacitor electrodes, 2D Mater. 7 (2020) 025010. https://doi.org/10.1088/2053-1583/ab6706.

[157] F. Liu, J. Zhou, S. Wang, B. Wang, C. Shen, L. Wang, Q. Hu, Q. Huang, A. Zhou, Preparation of High-Purity V_2C MXene and Electrochemical Properties as Li-Ion Batteries, J. Electrochem. Soc. 164 (2017) A709–A713. https://doi.org/10.1149/2.0641704jes.

[158] X. Wang, S. Lin, H. Tong, Y. Huang, P. Tong, B. Zhao, J. Dai, C. Liang, H. Wang, X. Zhu, Y. Sun, S. Dou, Two-dimensional V4C3 MXene as high performance electrode materials for supercapacitors, Electrochimica Acta. 307 (2019) 414–421. https://doi.org/10.1016/j.electacta.2019.03.205.

[159] Y. Wang, W. Zheng, P. Zhang, W. Tian, J. Chen, Z. Sun, Preparation of (Vx, Ti1−x)2C MXenes and their performance as anode materials for LIBs, J. Mater. Sci. 54 (2019) 11991–11999. https://doi.org/10.1007/s10853-019-03756-6.

[160] M. Naguib, O. Mashtalir, J. Carle, V. Presser, J. Lu, L. Hultman, Y. Gogotsi, M.W. Barsoum, Two-Dimensional Transition Metal Carbides, ACS Nano. 6 (2012) 1322–1331. https://doi.org/10.1021/nn204153h.

[161] M. Khazaei, M. Arai, T. Sasaki, C.-Y. Chung, N.S. Venkataramanan, M. Estili, Y. Sakka, Y. Kawazoe, Novel Electronic and Magnetic Properties of Two-Dimensional Transition Metal Carbides and Nitrides, Adv. Funct. Mater. 23 (2013) 2185–2192. https://doi.org/10.1002/adfm.201202502.

[162] H. Xiang, H. Lin, L. Yu, Y. Chen, Hypoxia-Irrelevant Photonic Thermodynamic Cancer Nanomedicine, ACS Nano. (2019) acsnano.8b08910. https://doi.org/10.1021/acsnano.8b08910.

[163] T. Su, R. Peng, Z.D. Hood, M. Naguib, I.N. Ivanov, J.K. Keum, Z. Qin, Z. Guo, Z. Wu, One-Step Synthesis of Nb_2O_5/C/Nb_2C (MXene) Composites and Their Use as Photocatalysts for Hydrogen Evolution, ChemSusChem. 11 (2018) 688–699. https://doi.org/10.1002/cssc.201702317.

[164] M. Naguib, J. Halim, J. Lu, K.M. Cook, L. Hultman, Y. Gogotsi, M.W. Barsoum, New Two-Dimensional Niobium and Vanadium Carbides as Promising Materials for Li-Ion Batteries, J. Am. Chem. Soc. 135 (2013) 15966–15969. https://doi.org/10.1021/ja405735d.

[165] J. Xiao, J. Wen, J. Zhao, X. Ma, H. Gao, X. Zhang, A safe etching route to synthesize highly crystalline Nb2CTx MXene for high performance asymmetric supercapacitor applications, Electrochimica Acta. 337 (2020) 135803. https://doi.org/10.1016/j.electacta.2020.135803.

[166] M. Ghidiu, M. Naguib, C. Shi, O. Mashtalir, L.M. Pan, B. Zhang, J. Yang, Y. Gogotsi, S.J.L. Billinge, M.W. Barsoum, Synthesis and characterization of two-dimensional Nb $_4$ C $_3$ (MXene), Chem Commun. 50 (2014) 9517–9520. https://doi.org/10.1039/C4CC03366C.
[167] C. Peng, P. Wei, X. Chen, Y. Zhang, F. Zhu, Y. Cao, H. Wang, H. Yu, F. Peng, A hydrothermal etching route to synthesis of 2D MXene (Ti3C2, Nb2C): Enhanced exfoliation and improved adsorption performance, Ceram. Int. 44 (2018) 18886–18893. https://doi.org/10.1016/j.ceramint.2018.07.124.
[168] J. Yang, M. Naguib, M. Ghidiu, L.-M. Pan, J. Gu, J. Nanda, J. Halim, Y. Gogotsi, M.W. Barsoum, Two-Dimensional Nb-Based M $_4$ C $_3$ Solid Solutions (MXenes), J. Am. Ceram. Soc. 99 (2016) 660–666. https://doi.org/10.1111/jace.13922.
[169] P. Cai, Q. He, L. Wang, X. Liu, J. Yin, Y. Liu, Y. Huang, Z. Huang, Two-dimensional Nb-based M4C3Tx MXenes and their sodium storage performances, Ceram. Int. 45 (2019) 5761–5767. https://doi.org/10.1016/j.ceramint.2018.12.042.
[170] Z. Yang, Y. Zheng, W. Li, J. Zhang, Investigation of two-dimensional hf-based MXenes as the anode materials for li/na-ion batteries: A DFT study, J. Comput. Chem. 40 (2019) 1352–1359. https://doi.org/10.1002/jcc.25789.
[171] H. Prats, H. McAloone, F. Viñes, F. Illas, Ultra-high selectivity biogas upgrading through porous MXenes, J. Mater. Chem. A. 8 (2020) 12296–12300. https://doi.org/10.1039/D0TA04522E.
[172] S. Sarikurt, D. Çakır, M. Keçeli, C. Sevik, The influence of surface functionalization on thermal transport and thermoelectric properties of MXene monolayers, Nanoscale. 10 (2018) 8859–8868. https://doi.org/10.1039/C7NR09144C.
[173] J.D. Gouveia, Á. Morales-García, F. Viñes, F. Illas, J.R.B. Gomes, MXenes as promising catalysts for water dissociation, Appl. Catal. B Environ. 260 (2020) 118191. https://doi.org/10.1016/j.apcatb.2019.118191.
[174] Z. Guo, J. Zhou, L. Zhu, Z. Sun, MXene: a promising photocatalyst for water splitting, J. Mater. Chem. A. 4 (2016) 11446–11452. https://doi.org/10.1039/C6TA04414J.
[175] X.-H. Zha, J. Zhou, K. Luo, J. Lang, Q. Huang, X. Zhou, J.S. Francisco, J. He, S. Du, Controllable magnitude and anisotropy of the electrical conductivity of Hf $_3$ C $_2$ O $_2$ MXene, J. Phys. Condens. Matter. 29 (2017) 165701. https://doi.org/10.1088/1361-648X/aa62da.
[176] C. Si, J. You, W. Shi, J. Zhou, Z. Sun, Quantum spin Hall phase in Mo $_2$ M $_2$ C $_3$ O $_2$ (M = Ti, Zr, Hf) MXenes, J. Mater. Chem. C. 4 (2016) 11524–11529. https://doi.org/10.1039/C6TC04560J.
[177] S. Zhao, W. Kang, J. Xue, Manipulation of electronic and magnetic properties of M $_2$ C (M = Hf, Nb, Sc, Ta, Ti, V, Zr) monolayer by applying mechanical strains, Appl. Phys. Lett. 104 (2014) 133106. https://doi.org/10.1063/1.4870515.
[178] J. Zhou, X. Zha, X. Zhou, F. Chen, G. Gao, S. Wang, C. Shen, T. Chen, C. Zhi, P. Eklund, S. Du, J. Xue, W. Shi, Z. Chai, Q. Huang, Synthesis and Electrochemical Properties of Two-Dimensional Hafnium Carbide, ACS Nano. 11 (2017) 3841–3850. https://doi.org/10.1021/acsnano.7b00030.
[179] B. Anasori, Y. Xie, M. Beidaghi, J. Lu, B.C. Hosler, L. Hultman, P.R.C. Kent, Y. Gogotsi, M.W. Barsoum, Two-Dimensional, Ordered, Double Transition Metals Carbides (MXenes), ACS Nano. 9 (2015) 9507–9516. https://doi.org/10.1021/acsnano.5b03591.
[180] X. Zou, H. Liu, H. Xu, X. Wu, X. Han, J. Kang, K.M. Reddy, A simple approach to synthesis Cr2CTx MXene for efficient hydrogen evolution reaction, Mater. Today Energy. 20 (2021) 100668. https://doi.org/10.1016/j.mtener.2021.100668.
[181] M.H. Tran, A.M. Malik, M. Dürrschnabel, A. Regoutz, P. Thakur, T.-L. Lee, D. Perera, L. Molina-Luna, K. Albe, J. Rohrer, C.S. Birkel, Experimental and theoretical investigation of the chemical exfoliation of Cr-based MAX phase particles, Dalton Trans. 49 (2020) 12215–12221. https://doi.org/10.1039/D0DT01448F.
[182] Q. Sun, Z. Fu, Z. Yang, Tunable magnetic and electronic properties of the Cr-based MXene (Cr2C) with functional groups and doping, J. Magn. Magn. Mater. 514 (2020) 167141. https://doi.org/10.1016/j.jmmm.2020.167141.
[183] J. Yang, S. Zhang, A. Wang, R. Wang, C.-K. Wang, G.-P. Zhang, L. Chen, High magnetoresistance in ultra-thin two-dimensional Cr-based MXenes, Nanoscale. 10 (2018) 19492–19497. https://doi.org/10.1039/C8NR04978E.
[184] C. Dai, Y. Chen, X. Jing, L. Xiang, D. Yang, H. Lin, Z. Liu, X. Han, R. Wu, Two-Dimensional Tantalum Carbide (MXenes) Composite Nanosheets for Multiple Imaging-Guided Photothermal Tumor Ablation, ACS Nano. 11 (2017) 12696–12712. https://doi.org/10.1021/acsnano.7b07241.
[185] H. Lin, Y. Wang, S. Gao, Y. Chen, J. Shi, Theranostic 2D Tantalum Carbide (MXene), Adv. Mater. 30 (2018) 1703284. https://doi.org/10.1002/adma.201703284.
[186] Z. Liu, H. Lin, M. Zhao, C. Dai, S. Zhang, W. Peng, Y. Chen, 2D Superparamagnetic Tantalum Carbide Composite MXenes for Efficient Breast-Cancer Theranostics, Theranostics. 8 (2018) 1648–1664. https://doi.org/10.7150/thno.23369.

[187] R. Syamsai, J.R. Rodriguez, V.G. Pol, Q. Van Le, K.M. Batoo, S.A. Farooq, S. Pandiaraj, M.R. Muthumareeswaran, E.H. Raslan, A.N. Grace, Double transition metal MXene (TixTa4−xC3) 2D materials as anodes for Li-ion batteries, Sci. Rep. 11 (2021) 688. https://doi.org/10.1038/s41598-020-79991-8.

[188] N.K. Chaudhari, H. Jin, B. Kim, D. San Baek, S.H. Joo, K. Lee, MXene: an emerging two-dimensional material for future energy conversion and storage applications, J. Mater. Chem. A. 5 (2017) 24564–24579. https://doi.org/10.1039/C7TA09094C.

[189] M. Naguib, M. Kurtoglu, V. Presser, J. Lu, J. Niu, M. Heon, L. Hultman, Y. Gogotsi, M.W. Barsoum, Two-Dimensional Nanocrystals Produced by Exfoliation of Ti3AlC2, Adv. Mater. 23 (2011) 4248–4253. https://doi.org/10.1002/adma.201102306.

[190] Q. Tang, Z. Zhou, P. Shen, Are MXenes Promising Anode Materials for Li Ion Batteries? Computational Studies on Electronic Properties and Li Storage Capability of Ti_3C_2 and $Ti_3C_2X_2$ (X = F, OH) Monolayer, J. Am. Chem. Soc. 134 (2012) 16909–16916. https://doi.org/10.1021/ja308463r.

[191] M. Naguib, J. Halim, J. Lu, K.M. Cook, L. Hultman, Y. Gogotsi, M.W. Barsoum, New Two-Dimensional Niobium and Vanadium Carbides as Promising Materials for Li-Ion Batteries, J. Am. Chem. Soc. 135 (2013) 15966–15969. https://doi.org/10.1021/ja405735d.

[192] I. Persson, J. Halim, H. Lind, T.W. Hansen, J.B. Wagner, L.-Å. Näslund, V. Darakchieva, J. Palisaitis, J. Rosen, P.O.Å. Persson, 2D Transition Metal Carbides (MXenes) for Carbon Capture, Adv. Mater. 31 (2019) 1805472. https://doi.org/10.1002/adma.201805472.

[193] K. Hantanasirisakul, Y. Gogotsi, Electronic and Optical Properties of 2D Transition Metal Carbides and Nitrides (MXenes), Adv. Mater. 30 (2018) 1804779. https://doi.org/10.1002/adma.201804779.

[194] X. Zang, W. Chen, X. Zou, J.N. Hohman, L. Yang, B. Li, M. Wei, C. Zhu, J. Liang, M. Sanghadasa, J. Gu, L. Lin, Self-Assembly of Large-Area 2D Polycrystalline Transition Metal Carbides for Hydrogen Electrocatalysis, Adv. Mater. 30 (2018) 1805188. https://doi.org/10.1002/adma.201805188.

[195] Z. Li, Z. Zhuang, F. Lv, H. Zhu, L. Zhou, M. Luo, J. Zhu, Z. Lang, S. Feng, W. Chen, L. Mai, S. Guo, The Marriage of the FeN_4 Moiety and MXene Boosts Oxygen Reduction Catalysis: Fe 3d Electron Delocalization Matters, Adv. Mater. 30 (2018) 1803220. https://doi.org/10.1002/adma.201803220.

[196] C. Eames, M.S. Islam, Ion Intercalation into Two-Dimensional Transition-Metal Carbides: Global Screening for New High-Capacity Battery Materials, J. Am. Chem. Soc. 136 (2014) 16270–16276. https://doi.org/10.1021/ja508154e.

[197] M. Naguib, J. Come, B. Dyatkin, V. Presser, P.-L. Taberna, P. Simon, M.W. Barsoum, Y. Gogotsi, MXene: a promising transition metal carbide anode for lithium-ion batteries, Electrochem. Commun. 16 (2012) 61–64. https://doi.org/10.1016/j.elecom.2012.01.002.

[198] M. Naguib, J. Come, B. Dyatkin, V. Presser, P.-L. Taberna, P. Simon, M.W. Barsoum, Y. Gogotsi, MXene: a promising transition metal carbide anode for lithium-ion batteries, Electrochem. Commun. 16 (2012) 61–64. https://doi.org/10.1016/j.elecom.2012.01.002.

[199] Y. Xie, Y. Dall'Agnese, M. Naguib, Y. Gogotsi, M.W. Barsoum, H.L. Zhuang, P.R.C. Kent, Prediction and Characterization of MXene Nanosheet Anodes for Non-Lithium-Ion Batteries, ACS Nano. 8 (2014) 9606–9615. https://doi.org/10.1021/nn503921j.

[200] O. Mashtalir, M.R. Lukatskaya, M.-Q. Zhao, M.W. Barsoum, Y. Gogotsi, Amine-Assisted Delamination of Nb_2C MXene for Li-Ion Energy Storage Devices, Adv. Mater. 27 (2015) 3501–3506. https://doi.org/10.1002/adma.201500604.

[201] Z. Fu, N. Wang, D. Legut, C. Si, Q. Zhang, S. Du, T.C. Germann, J.S. Francisco, R. Zhang, Rational Design of Flexible Two-Dimensional MXenes with Multiple Functionalities, Chem. Rev. 119 (2019) 11980–12031. https://doi.org/10.1021/acs.chemrev.9b00348.

[202] J. Luo, X. Tao, J. Zhang, Y. Xia, H. Huang, L. Zhang, Y. Gan, C. Liang, W. Zhang, Sn^{4+} Ion Decorated Highly Conductive Ti_3C_2 MXene: Promising Lithium-Ion Anodes with Enhanced Volumetric Capacity and Cyclic Performance, ACS Nano. 10 (2016) 2491–2499. https://doi.org/10.1021/acsnano.5b07333.

[203] D. Sun, Q. Hu, J. Chen, X. Zhang, L. Wang, Q. Wu, A. Zhou, Structural Transformation of MXene (V_2C, Cr_2C, and Ta_2C) with O Groups during Lithiation: A First-Principles Investigation, ACS Appl. Mater. Interfaces. 8 (2016) 74–81. https://doi.org/10.1021/acsami.5b03863.

[204] C.E. Ren, M. Zhao, T. Makaryan, J. Halim, M. Boota, S. Kota, B. Anasori, M.W. Barsoum, Y. Gogotsi, Porous Two-Dimensional Transition Metal Carbide (MXene) Flakes for High-Performance Li-Ion Storage, ChemElectroChem. 3 (2016) 689–693. https://doi.org/10.1002/celc.201600059.

[205] Z. Lin, D. Sun, Q. Huang, J. Yang, M.W. Barsoum, X. Yan, Carbon nanofiber bridged two-dimensional titanium carbide as a superior anode for lithium-ion batteries, J. Mater. Chem. A. 3 (2015) 14096–14100. https://doi.org/10.1039/C5TA01855B.

[206] Y.-T. Liu, P. Zhang, N. Sun, B. Anasori, Q.-Z. Zhu, H. Liu, Y. Gogotsi, B. Xu, Self-Assembly of Transition Metal Oxide Nanostructures on MXene Nanosheets for Fast and Stable Lithium Storage, Adv. Mater. 30 (2018) 1707334. https://doi.org/10.1002/adma.201707334.

[207] B. Ahmed, D.H. Anjum, Y. Gogotsi, H.N. Alshareef, Atomic layer deposition of SnO 2 on MXene for Li-ion battery anodes, Nano Energy. 34 (2017) 249–256. https://doi.org/10.1016/j.nanoen.2017.02.043.
[208] C.J. Zhang, S.J. Kim, M. Ghidiu, M.-Q. Zhao, M.W. Barsoum, V. Nicolosi, Y. Gogotsi, Layered Orthorhombic Nb_2O_5@$Nb_4C_3T_x$ and TiO_2@$Ti_3C_2T_x$ Hierarchical Composites for High Performance Li-ion Batteries, Adv. Funct. Mater. 26 (2016) 4143–4151. https://doi.org/10.1002/adfm.201600682.
[209] G. Zou, Z. Zhang, J. Guo, B. Liu, Q. Zhang, C. Fernandez, Q. Peng, Synthesis of MXene/Ag Composites for Extraordinary Long Cycle Lifetime Lithium Storage at High Rates, ACS Appl. Mater. Interfaces. 8 (2016) 22280–22286. https://doi.org/10.1021/acsami.6b08089.
[210] J. Nan, X. Guo, J. Xiao, X. Li, W. Chen, W. Wu, H. Liu, Y. Wang, M. Wu, G. Wang, Nanoengineering of 2D MXene-Based Materials for Energy Storage Applications, Small. 17 (2021) 1902085. https://doi.org/10.1002/smll.201902085.
[211] A. Manthiram, S.-H. Chung, C. Zu, Lithium-Sulfur Batteries: Progress and Prospects, Adv. Mater. 27 (2015) 1980–2006. https://doi.org/10.1002/adma.201405115.
[212] K. Chen, J. Cao, Q. Lu, Q. Wang, M. Yao, M. Han, Z. Niu, J. Chen, Sulfur nanoparticles encapsulated in reduced graphene oxide nanotubes for flexible lithium-sulfur batteries, Nano Res. 11 (2018) 1345–1357. https://doi.org/10.1007/s12274-017-1749-2.
[213] J. Liang, Z.-H. Sun, F. Li, H.-M. Cheng, Carbon materials for Li–S batteries: Functional evolution and performance improvement, Energy Storage Mater. 2 (2016) 76–106. https://doi.org/10.1016/j.ensm.2015.09.007.
[214] J. Song, C. Zhang, X. Guo, J. Zhang, L. Luo, H. Liu, F. Wang, G. Wang, Entrapping polysulfides by using ultrathin hollow carbon sphere-functionalized separators in high-rate lithium-sulfur batteries, J. Mater. Chem. A. 6 (2018) 16610–16616. https://doi.org/10.1039/C8TA04800B.
[215] A. Rosenman, E. Markevich, G. Salitra, D. Aurbach, A. Garsuch, F.F. Chesneau, Review on Li-Sulfur Battery Systems: an Integral Perspective, Adv. Energy Mater. 5 (2015) 1500212. https://doi.org/10.1002/aenm.201500212.
[216] M. Wild, L. O'Neill, T. Zhang, R. Purkayastha, G. Minton, M. Marinescu, G.J. Offer, Lithium sulfur batteries, a mechanistic review, Energy Environ. Sci. 8 (2015) 3477–3494. https://doi.org/10.1039/C5EE01388G.
[217] Q. Zhang, Y. Wang, Z.W. Seh, Z. Fu, R. Zhang, Y. Cui, Understanding the Anchoring Effect of Two-Dimensional Layered Materials for Lithium–Sulfur Batteries, Nano Lett. 15 (2015) 3780–3786. https://doi.org/10.1021/acs.nanolett.5b00367.
[218] Q. Zhao, Q. Zhu, Y. Liu, B. Xu, Status and Prospects of MXene-Based Lithium–Sulfur Batteries, Adv. Funct. Mater. 31 (2021) 2100457. https://doi.org/10.1002/adfm.202100457.
[219] E.S. Sim, G.S. Yi, M. Je, Y. Lee, Y.-C. Chung, Understanding the anchoring behavior of titanium carbide-based MXenes depending on the functional group in Li S batteries: A density functional theory study, J. Power Sources. 342 (2017) 64–69. https://doi.org/10.1016/j.jpowsour.2016.12.042.
[220] X. Zhao, M. Liu, Y. Chen, B. Hou, N. Zhang, B. Chen, N. Yang, K. Chen, J. Li, L. An, Fabrication of layered Ti_3C_2 with an accordion-like structure as a potential cathode material for high performance lithium–sulfur batteries, J. Mater. Chem. A. 3 (2015) 7870–7876. https://doi.org/10.1039/C4TA07101H.
[221] X. Liang, A. Garsuch, L.F. Nazar, Sulfur Cathodes Based on Conductive MXene Nanosheets for High-Performance Lithium-Sulfur Batteries, Angew. Chem. Int. Ed. 54 (2015) 3907–3911. https://doi.org/10.1002/anie.201410174.
[222] C. Xiong, G.Y. Zhu, H.R. Jiang, Q. Chen, T.S. Zhao, Achieving multiplexed functionality in a hierarchical MXene-based sulfur host for high-rate, high-loading lithium-sulfur batteries, Energy Storage Mater. 33 (2020) 147–157. https://doi.org/10.1016/j.ensm.2020.08.006.
[223] X. Liang, Y. Rangom, C.Y. Kwok, Q. Pang, L.F. Nazar, Interwoven MXene Nanosheet/Carbon-Nanotube Composites as Li-S Cathode Hosts, Adv. Mater. 29 (2017) 1603040. https://doi.org/10.1002/adma.201603040.
[224] B. Zhang, C. Luo, G. Zhou, Z. Pan, J. Ma, H. Nishihara, Y. He, F. Kang, W. Lv, Q. Yang, Lamellar MXene Composite Aerogels with Sandwiched Carbon Nanotubes Enable Stable Lithium–Sulfur Batteries with a High Sulfur Loading, Adv. Funct. Mater. 31 (2021) 2100793. https://doi.org/10.1002/adfm.202100793.
[225] L.-W. Lin, M. Qi, Z.-T. Bai, S.-X. Yan, Z.-Y. Sui, B.-H. Han, Y.-W. Liu, Crumpled nitrogen-doped aerogels derived from MXene and pyrrole-formaldehyde as modified separators for stable lithium-sulfur batteries, Appl. Surf. Sci. 555 (2021) 149717. https://doi.org/10.1016/j.apsusc.2021.149717.
[226] W. Bao, L. Liu, C. Wang, S. Choi, D. Wang, G. Wang, Facile Synthesis of Crumpled Nitrogen-Doped MXene Nanosheets as a New Sulfur Host for Lithium-Sulfur Batteries, Adv. Energy Mater. 8 (2018) 1702485. https://doi.org/10.1002/aenm.201702485.
[227] L. Ma, H. Yuan, W. Zhang, G. Zhu, Y. Wang, Y. Hu, P. Zhao, R. Chen, T. Chen, J. Liu, Z. Hu, Z. Jin, Porous-Shell Vanadium Nitride Nanobubbles with Ultrahigh Areal Sulfur Loading for High-Capacity

and Long-Life Lithium–Sulfur Batteries, Nano Lett. 17 (2017) 7839–7846. https://doi.org/10.1021/acs.nanolett.7b04084.

[228] M. Wang, Q. Liang, J. Han, Y. Tao, D. Liu, C. Zhang, W. Lv, Q.-H. Yang, Catalyzing polysulfide conversion by g-C3N4 in a graphene network for long-life lithium-sulfur batteries, Nano Res. 11 (2018) 3480–3489. https://doi.org/10.1007/s12274-018-2023-y.

[229] W. Bao, D. Su, W. Zhang, X. Guo, G. Wang, 3D Metal Carbide@Mesoporous Carbon Hybrid Architecture as a New Polysulfide Reservoir for Lithium-Sulfur Batteries, Adv. Funct. Mater. 26 (2016) 8746–8756. https://doi.org/10.1002/adfm.201603704.

[230] J. Song, D. Su, X. Xie, X. Guo, W. Bao, G. Shao, G. Wang, Immobilizing Polysulfides with MXene-Functionalized Separators for Stable Lithium–Sulfur Batteries, ACS Appl. Mater. Interfaces. 8 (2016) 29427–29433. https://doi.org/10.1021/acsami.6b09027.

[231] D. Rao, L. Zhang, Y. Wang, Z. Meng, X. Qian, J. Liu, X. Shen, G. Qiao, R. Lu, Mechanism on the Improved Performance of Lithium Sulfur Batteries with MXene-Based Additives, J. Phys. Chem. C. 121 (2017) 11047–11054. https://doi.org/10.1021/acs.jpcc.7b00492.

[232] Y. Dong, S. Zheng, J. Qin, X. Zhao, H. Shi, X. Wang, J. Chen, Z.-S. Wu, All-MXene-Based Integrated Electrode Constructed by Ti_3C_2 Nanoribbon Framework Host and Nanosheet Interlayer for High-Energy-Density Li–S Batteries, ACS Nano. 12 (2018) 2381–2388. https://doi.org/10.1021/acsnano.7b07672.

[233] D. Zhang, S. Wang, R. Hu, J. Gu, Y. Cui, B. Li, W. Chen, C. Liu, J. Shang, S. Yang, Catalytic Conversion of Polysulfides on Single Atom Zinc Implanted MXene toward High-Rate Lithium–Sulfur Batteries, Adv. Funct. Mater. 30 (2020) 2002471. https://doi.org/10.1002/adfm.202002471.

[234] C. Wen, X. Zheng, X. Li, M. Yuan, H. Li, G. Sun, Rational design of 3D hierarchical MXene@AlF3/Ni(OH)2 nanohybrid for high-performance lithium-sulfur batteries, Chem. Eng. J. 409 (2021) 128102. https://doi.org/10.1016/j.cej.2020.128102.

[235] S.-Y. Qiu, C. Wang, Z.-X. Jiang, L.-S. Zhang, L.-L. Gu, K.-X. Wang, J. Gao, X.-D. Zhu, G. Wu, Rational design of MXene@TiO_2 nanoarray enabling dual lithium polysulfide chemisorption towards high-performance lithium–sulfur batteries, Nanoscale. 12 (2020) 16678–16684. https://doi.org/10.1039/D0NR03528A.

[236] P.E. Lokhande, U.S. Chavan, A. Pandey, Materials and Fabrication Methods for Electrochemical Supercapacitors: Overview, Electrochem. Energy Rev. 3 (2020) 155–186. https://doi.org/10.1007/s41918-019-00057-z.

[237] A. VahidMohammadi, M. Mojtabavi, N.M. Caffrey, M. Wanunu, M. Beidaghi, Assembling 2D MXenes into Highly Stable Pseudocapacitive Electrodes with High Power and Energy Densities, Adv. Mater. 31 (2019) 1806931. https://doi.org/10.1002/adma.201806931.

[238] P.E. Lokhande, U.S. Chavan, Nanoflower-like Ni(OH)2 synthesis with chemical bath deposition method for high performance electrochemical applications, Mater. Lett. 218 (2018) 225–228. https://doi.org/10.1016/j.matlet.2018.02.012.

[239] P.E. Lokhande, U.S. Chavan, All-Solid-State Asymmetric Supercapacitor Based on Ni–Co Layered Double Hydroxide and rGO Nanocomposite Deposited on Ni Foam, J. Electrochem. Energy Convers. Storage. 17 (2020) 031013. https://doi.org/10.1115/1.4045977.

[240] Y. Wang, Y. Song, Y. Xia, Electrochemical capacitors: mechanism, materials, systems, characterization and applications, Chem. Soc. Rev. 45 (2016) 5925–5950. https://doi.org/10.1039/C5CS00580A.

[241] M. Hu, H. Zhang, T. Hu, B. Fan, X. Wang, Z. Li, Emerging 2D MXenes for supercapacitors: status, challenges and prospects, Chem. Soc. Rev. 49 (2020) 6666–6693. https://doi.org/10.1039/D0CS00175A.

[242] Z. Lin, E. Goikolea, A. Balducci, K. Naoi, P.L. Taberna, M. Salanne, G. Yushin, P. Simon, Materials for supercapacitors: When Li-ion battery power is not enough, Mater. Today. 21 (2018) 419–436. https://doi.org/10.1016/j.mattod.2018.01.035.

[243] M. Hu, H. Zhang, T. Hu, B. Fan, X. Wang, Z. Li, Emerging 2D MXenes for supercapacitors: status, challenges and prospects, Chem. Soc. Rev. 49 (2020) 6666–6693. https://doi.org/10.1039/D0CS00175A.

[244] M.R. Lukatskaya, O. Mashtalir, C.E. Ren, Y. Dall'Agnese, P. Rozier, P.L. Taberna, M. Naguib, P. Simon, M.W. Barsoum, Y. Gogotsi, Cation Intercalation and High Volumetric Capacitance of Two-Dimensional Titanium Carbide, Science. 341 (2013) 1502–1505. https://doi.org/10.1126/science.1241488.

[245] M.D. Levi, M.R. Lukatskaya, S. Sigalov, M. Beidaghi, N. Shpigel, L. Daikhin, D. Aurbach, M.W. Barsoum, Y. Gogotsi, Solving the Capacitive Paradox of 2D MXene using Electrochemical Quartz-Crystal Admittance and In Situ Electronic Conductance Measurements, Adv. Energy Mater. 5 (2015) 1400815. https://doi.org/10.1002/aenm.201400815.

[246] B. Anasori, M.R. Lukatskaya, Y. Gogotsi, 2D metal carbides and nitrides (MXenes) for energy storage, Nat. Rev. Mater. 2 (2017) 16098. https://doi.org/10.1038/natrevmats.2016.98.

[247] M.R. Lukatskaya, S.-M. Bak, X. Yu, X.-Q. Yang, M.W. Barsoum, Y. Gogotsi, Probing the Mechanism of High Capacitance in 2D Titanium Carbide Using In Situ X-Ray Absorption Spectroscopy, Adv. Energy Mater. 5 (2015) 1500589. https://doi.org/10.1002/aenm.201500589.
[248] J. Guo, Q. Peng, H. Fu, G. Zou, Q. Zhang, Heavy-Metal Adsorption Behavior of Two-Dimensional Alkalization-Intercalated MXene by First-Principles Calculations, J. Phys. Chem. C. 119 (2015) 20923–20930. https://doi.org/10.1021/acs.jpcc.5b05426.
[249] L. Ma, T. Zhao, F. Xu, T. You, X. Zhang, A dual utilization strategy of lignosulfonate for MXene asymmetric supercapacitor with high area energy density, Chem. Eng. J. 405 (2021) 126694. https://doi.org/10.1016/j.cej.2020.126694.
[250] K. Xu, X. Ji, B. Zhang, C. Chen, Y. Ruan, L. Miao, J. Jiang, Charging/Discharging Dynamics in Two-Dimensional Titanium Carbide (MXene) Slit Nanopore: Insights from molecular dynamic study, Electrochimica Acta. 196 (2016) 75–83. https://doi.org/10.1016/j.electacta.2016.02.165.
[251] O. Mashtalir, M.R. Lukatskaya, A.I. Kolesnikov, E. Raymundo-Piñero, M. Naguib, M.W. Barsoum, Y. Gogotsi, The effect of hydrazine intercalation on the structure and capacitance of 2D titanium carbide (MXene), Nanoscale. 8 (2016) 9128–9133. https://doi.org/10.1039/C6NR01462C.
[252] M. Ghidiu, M.R. Lukatskaya, M.-Q. Zhao, Y. Gogotsi, M.W. Barsoum, Conductive two-dimensional titanium carbide 'clay' with high volumetric capacitance, Nature. 516 (2014) 78–81. https://doi.org/10.1038/nature13970.
[253] J. Tang, T. Mathis, X. Zhong, X. Xiao, H. Wang, M. Anayee, F. Pan, B. Xu, Y. Gogotsi, Optimizing Ion Pathway in Titanium Carbide MXene for Practical High-Rate Supercapacitor, Adv. Energy Mater. 11 (2021) 2003025. https://doi.org/10.1002/aenm.202003025.
[254] Y.-Y. Peng, B. Akuzum, N. Kurra, M.-Q. Zhao, M. Alhabeb, B. Anasori, E.C. Kumbur, H.N. Alshareef, M.-D. Ger, Y. Gogotsi, All-MXene (2D titanium carbide) solid-state microsupercapacitors for on-chip energy storage, Energy Environ. Sci. 9 (2016) 2847–2854. https://doi.org/10.1039/C6EE01717G.
[255] N. Jäckel, B. Krüner, K.L. Van Aken, M. Alhabeb, B. Anasori, F. Kaasik, Y. Gogotsi, V. Presser, Electrochemical in Situ Tracking of Volumetric Changes in Two-Dimensional Metal Carbides (MXenes) in Ionic Liquids, ACS Appl. Mater. Interfaces. 8 (2016) 32089–32093. https://doi.org/10.1021/acsami.6b11744.
[256] M. Boota, M. Pasini, F. Galeotti, W. Porzio, M.-Q. Zhao, J. Halim, Y. Gogotsi, Interaction of Polar and Nonpolar Polyfluorenes with Layers of Two-Dimensional Titanium Carbide (MXene): Intercalation and Pseudocapacitance, Chem. Mater. 29 (2017) 2731–2738. https://doi.org/10.1021/acs.chemmater.6b03933.
[257] Y. Xia, T.S. Mathis, M.-Q. Zhao, B. Anasori, A. Dang, Z. Zhou, H. Cho, Y. Gogotsi, S. Yang, Thickness-independent capacitance of vertically aligned liquid-crystalline MXenes, Nature. 557 (2018) 409–412. https://doi.org/10.1038/s41586-018-0109-z.
[258] J. Li, X. Yuan, C. Lin, Y. Yang, L. Xu, X. Du, J. Xie, J. Lin, J. Sun, Achieving High Pseudocapacitance of 2D Titanium Carbide (MXene) by Cation Intercalation and Surface Modification, Adv. Energy Mater. 7 (2017) 1602725. https://doi.org/10.1002/aenm.201602725.
[259] H. Wang, Y. Wu, J. Zhang, G. Li, H. Huang, X. Zhang, Q. Jiang, Enhancement of the electrical properties of MXene Ti3C2 nanosheets by post-treatments of alkalization and calcination, Mater. Lett. 160 (2015) 537–540. https://doi.org/10.1016/j.matlet.2015.08.046.
[260] Y. Guan, S. Jiang, Y. Cong, J. Wang, Z. Dong, Q. Zhang, G. Yuan, Y. Li, X. Li, A hydrofluoric acid-free synthesis of 2D vanadium carbide (V_2C) MXene for supercapacitor electrodes, 2D Mater. 7 (2020) 025010. https://doi.org/10.1088/2053-1583/ab6706.
[261] M.R. Lukatskaya, S. Kota, Z. Lin, M.-Q. Zhao, N. Shpigel, M.D. Levi, J. Halim, P.-L. Taberna, M.W. Barsoum, P. Simon, Y. Gogotsi, Ultra-high-rate pseudocapacitive energy storage in two-dimensional transition metal carbides, Nat. Energy. 2 (2017) 17105. https://doi.org/10.1038/nenergy.2017.105.
[262] Z. Wang, Z. Xu, H. Huang, X. Chu, Y. Xie, D. Xiong, C. Yan, H. Zhao, H. Zhang, W. Yang, Unraveling and Regulating Self-Discharge Behavior of $Ti_3C_2T_x$ MXene-Based Supercapacitors, ACS Nano. 14 (2020) 4916–4924. https://doi.org/10.1021/acsnano.0c01056.
[263] E. Balcı, Ü.Ö. Akkuş, S. Berber, Band gap modification in doped MXene: Sc_2CF_2, J. Mater. Chem. C. 5 (2017) 5956–5961. https://doi.org/10.1039/C7TC01765K.
[264] Y. Wen, T.E. Rufford, X. Chen, N. Li, M. Lyu, L. Dai, L. Wang, Nitrogen-doped Ti 3 C 2 T x MXene electrodes for high-performance supercapacitors, Nano Energy. 38 (2017) 368–376. https://doi.org/10.1016/j.nanoen.2017.06.009.
[265] C. Yang, W. Que, X. Yin, Y. Tian, Y. Yang, M. Que, Improved capacitance of nitrogen-doped delaminated two-dimensional titanium carbide by urea-assisted synthesis, Electrochimica Acta. 225 (2017) 416–424. https://doi.org/10.1016/j.electacta.2016.12.173.
[266] K. Krishnamoorthy, P. Pazhamalai, S. Sahoo, S.-J. Kim, Titanium carbide sheet based high performance wire type solid state supercapacitors, J. Mater. Chem. A. 5 (2017) 5726–5736. https://doi.org/10.1039/C6TA11198J.

[267] M. Kurtoglu, M. Naguib, Y. Gogotsi, M.W. Barsoum, First principles study of two-dimensional early transition metal carbides, MRS Commun. 2 (2012) 133–137. https://doi.org/10.1557/mrc.2012.25.
[268] C.J. Zhang, B. Anasori, A. Seral-Ascaso, S.-H. Park, N. McEvoy, A. Shmeliov, G.S. Duesberg, J.N. Coleman, Y. Gogotsi, V. Nicolosi, Transparent, Flexible, and Conductive 2D Titanium Carbide (MXene) Films with High Volumetric Capacitance, Adv. Mater. 29 (2017) 1702678. https://doi.org/10.1002/adma.201702678.
[269] Y. Zhou, K. Maleski, B. Anasori, J.O. Thostenson, Y. Pang, Y. Feng, K. Zeng, C.B. Parker, S. Zauscher, Y. Gogotsi, J.T. Glass, C. Cao, $Ti_3C_2T_x$ MXene-Reduced Graphene Oxide Composite Electrodes for Stretchable Supercapacitors, ACS Nano. 14 (2020) 3576–3586. https://doi.org/10.1021/acsnano.9b10066.

Table captions

Table 1 Comparison of parameters used for various synthesis methods for MXene preparation also obtained products image and specialities of the used method.

Figure captions

Figure 1. MXene compositions reported to date. The top row shows structures of mono-M MXenes; the second row shows double-M solids solutions (SS) (green). The third-row shows ordered double-M MXenes (red). The fourth row shows an ordered di-vacancy structure, which has only been reported for the M2C MXenes, making a M1.33C composition due to 0.33 atom % of vacancies in the M layers (pink). [10] Reproduced with permission © 2019, Springer

Figure 2. List of the main synthesis and processing breakthroughs over the first 10 years of MXenes' research, the new MXene core compositions discovered in that decade (surface termination abbreviation T_x is omitted in the chemical formula for simplicity) and progress in surface terminations control. [56] Reproduced with permission, © 2021, Wiley Online Library

Figure 3. MXenes can have at least three different formulas: M2X, M3X2 and M4X3, where M is an early transition metal and X is carbon and/or nitrogen. They can be made in three different forms: mono-M elements (for example, Ti2C and Nb4C3);[57] Reproduced with permission, © 2017, Nature.

Figure 4. Configurations of functionalized MXenes with different arrangements of the surface atoms: side views of a) bare Ti_3C_2 b) I-$Ti_3C_2(OH)_2$ c) II- $Ti_3C_2(OH)_2$ and d) III- $Ti_3C_2(OH)_2$ e, f) top views of I- $Ti_3C_2(OH)_2$ and II- $Ti_3C_2(OH)_2$. [58] Reproduced with permission, © 2012, Elsevier.

Figure 5 a. Structure of MAX phases and the corresponding MXenes. [74] Reproduced with permission, © 2014, American Chemical Society. b. Schematic describing the synthesis process of MXenes from MAX phases. [8] Reproduced with permission, © 2012, American Chemical Society.

Figure 6 a. Schematic illustration of molten salt treatment [71] Reproduced with permission, © 2015, Nature **b.** Schematic illustration of UV-induced selective etching synthesis of two-dimensional (2D) mesoporous Mo_2C [72]

Reproduced with permission, ©2015, Royal Society of Chemistry **c.** Schematic of the reaction for hydrothermal method for MXene preparation [74] Reproduced with permission, © 2014, American Chemical Society.

Figure 7 **a.** PDOS and projected band structures for Ti_2CT_x[93]. Reproduced with permission, © 2014, American Chemical Society.

Figure 8 a. SEM images of Sn^{4+} decorated Ti_3C_2 and cyclic performance of nanocomposite [191] Reproduced with permission, © 2015, Wiley Online Library.

Figure 9 a. Schematic illustration for synthesis of S/L-Ti_3C_2 b-e. Representative FESEM micrographs of f. Schematic illustration Li-S discharge process g. Galvanostatic charge/discharge curves. [207] Reproduced with permission, © 2015, Royal Society of Chemistry.

Figure 10 a. Schematic illustrations of the etching process of $Ti_3C_2T_x$ nanosheets and the obtained hierarchical nanoporous structure b. The schematic illustration of the ion pathway optimization in S-etched Ti_3C_2Tx fillm comparing with the L-pristine film. c-g. Comparison of electrochemical performance of $Ti_3C_2T_x$ films before and after etching.[253] Reproduced with permission, © 2021, Wiley Online Library